

HASP 2014

Science Report of Payload # 7

University of North Florida and University of North Dakota



Development of free flying payload to measure ozone profile in the stratosphere and pollutant gases in atmosphere and troposphere using nanocrystalline sensors on a high altitude balloon platform

**Students Team:**

**Kenneth Emanuel (UNF) (Team Leader)**

**Brittany Nassau (UNF)**

**Faculty Advisors:**

**Dr. Nirmalkumar G. Patel**

Department of Physics, University of North Florida, Jacksonville, FL 32224

**and**

**Dr. Ron Fevig**

Department of Space Studies, University of North Dakota, Grand Forks, ND 58202

# Index

<b>Section #</b>	<b>Contents</b>	<b>Page #</b>
<b>1</b>	Introduction and Mission Objectives	<b>3</b>
<b>2</b>	Fabrication of Nanocrystalline Thin Film Gas Sensors	<b>7</b>
<b>3</b>	Working Principles of Gas Sensors	<b>11</b>
<b>4</b>	Calibration of Gas Sensors	<b>12</b>
<b>5</b>	Fabrication of Payload Body	<b>15</b>
<b>6</b>	Electronic Circuits	<b>26</b>
<b>7</b>	Integration of Payload and Thermal Vacuum Test	<b>31</b>
<b>8</b>	Launching of Payload	<b>34</b>
<b>9</b>	Results and Discussions	<b>38</b>
<b>9.1</b>	How ozone profile measured?	<b>38</b>
<b>9.2</b>	Balloon Flight Profile and Response of Pressure Sensor	<b>38</b>
<b>9.3</b>	Power Budget during the Flight	<b>40</b>
<b>9.4</b>	Thermal Stability of the Payload	<b>41</b>
<b>9.5</b>	Measurements of Photovoltage Profile during the Flight	<b>43</b>
<b>9.6</b>	Discussion of Response of Gas Sensors Profiles	<b>46</b>
<b>9.7</b>	Response of Ozone Sensors during the Flight	<b>49</b>
<b>9.8</b>	Measurements of ozone profile in the stratosphere and comparison with the theoretical profile	<b>55</b>
<b>10</b>	Problems, Failure Analysis and Future Plan	<b>61</b>
<b>11</b>	Conclusions	<b>61</b>
<b>12</b>	Acknowledgements	<b>62</b>

# 1. Introduction and Mission Objectives

After success of the HASP flights made during 2008 to 2013, University of North Dakota (UND) and University of North Florida (UNF) team decided to go for the HASP2014 balloon flight to measure the ozone profile in the stratosphere again using an improved version of payload consist of the nanocomposite ozone gas and reducing gases sensors, the pressure sensor, GPS and improved version of software and microcontroller circuit. About 90% of ozone is concentrated between 15 and 30 kilometers above the earth's surface (stratospheric ozone). It is also found at ground level in lower concentrations where it is a key component of smog over major cities (tropospheric ozone). The atmospheric layers defined by changes in temperature are shown in fig.1 (b), while the presence of ozone layer in the stratosphere is shown in fig. 1(b).

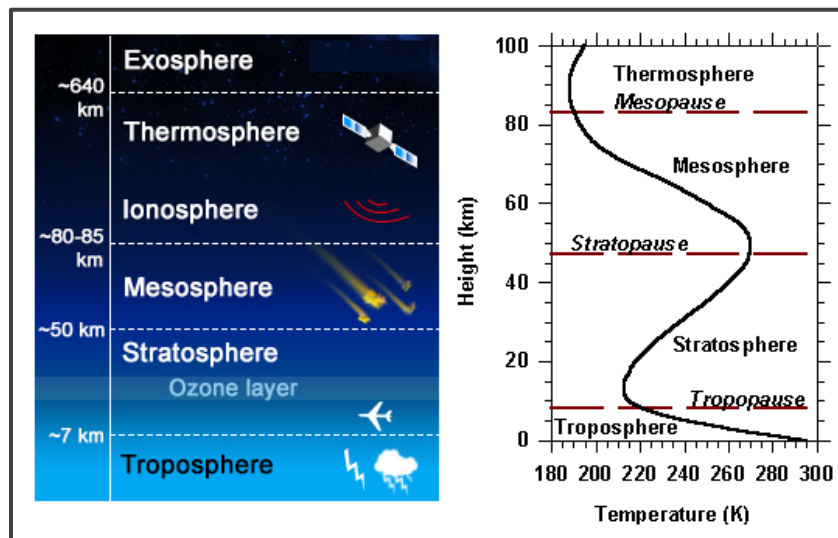


Fig.1 (a) shows the atmospheric layers defined by changes in temperature

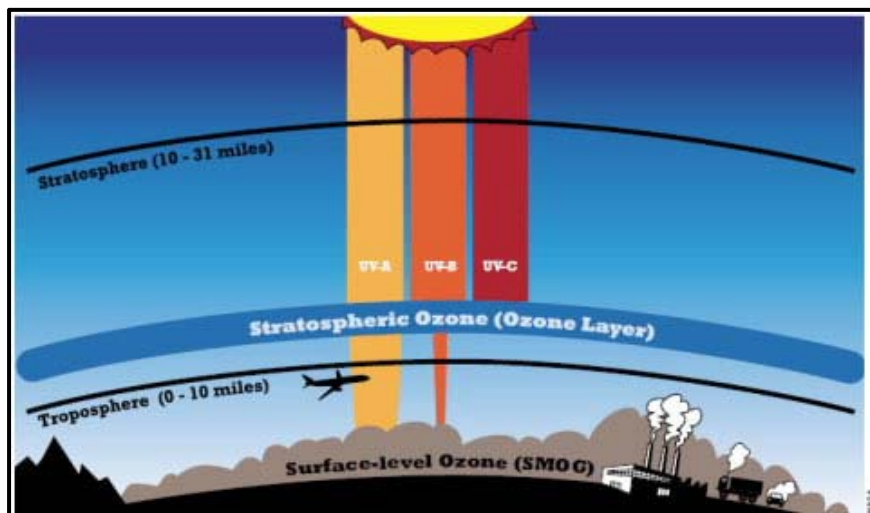
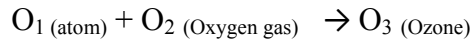
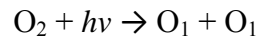
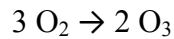


Fig.1 (b) The Ozone layer in the stratosphere: Our global sunscreen

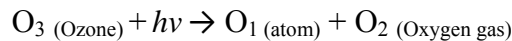
**Generation of Ozone in the Stratosphere:** Oxygen gas ( $O_2$ ) is present in the atmosphere. High energy or shorter wavelength UV light ( $h\nu$ ) collides with the oxygen molecule ( $O_2$ ), causing it to split into two oxygen atoms. These atoms are unstable, and they prefer being "bound" to something else. The free oxygen atoms then smash into other molecules of oxygen, forming ozone ( $O_3$ ).



The overall reaction between oxygen and ozone formation is:



The ozone is destroyed in the process that protects us from UV-B and UV-C rays emitted by the Sun. When ozone ( $O_3$ ) absorbs UV light ( $h\nu$ ), it will split the molecule into one free oxygen atom ( $O_1$ ) and one molecule of oxygen gas ( $O_2$ ). Thus, absorption of UV-B and UV-C leads to the destruction of ozone



Ozone is valuable to us because it absorbs harmful UV radiation during its destruction process (fig.2 (a)). A dynamic equilibrium is established in these reactions. The ozone concentration varies due to the amount of radiation of light received from the sun.

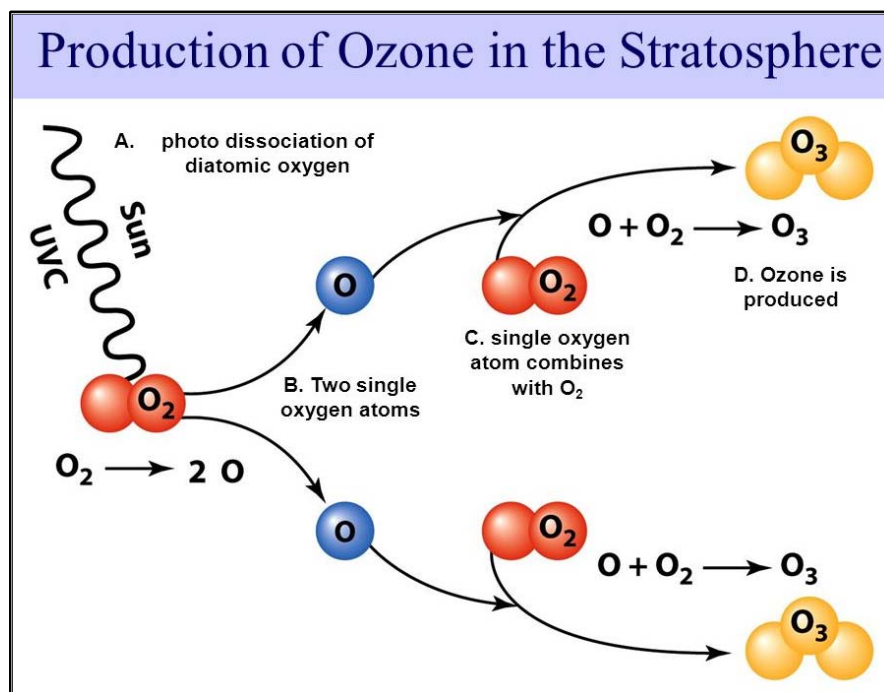


Fig.2 (a) Generation of ozone in the presence of UV light in stratosphere

**Generation of Ozone in the Troposphere:** Ozone in the troposphere is bad. It creates the respiratory problem, destroys polymers and reduces the plant growth. This ozone is contributing to the smog and greenhouse gases created by human activities, which is shown in fig.2 (b). Ozone close to the ground surface does not exist in high enough concentrations to shield us from UV light.

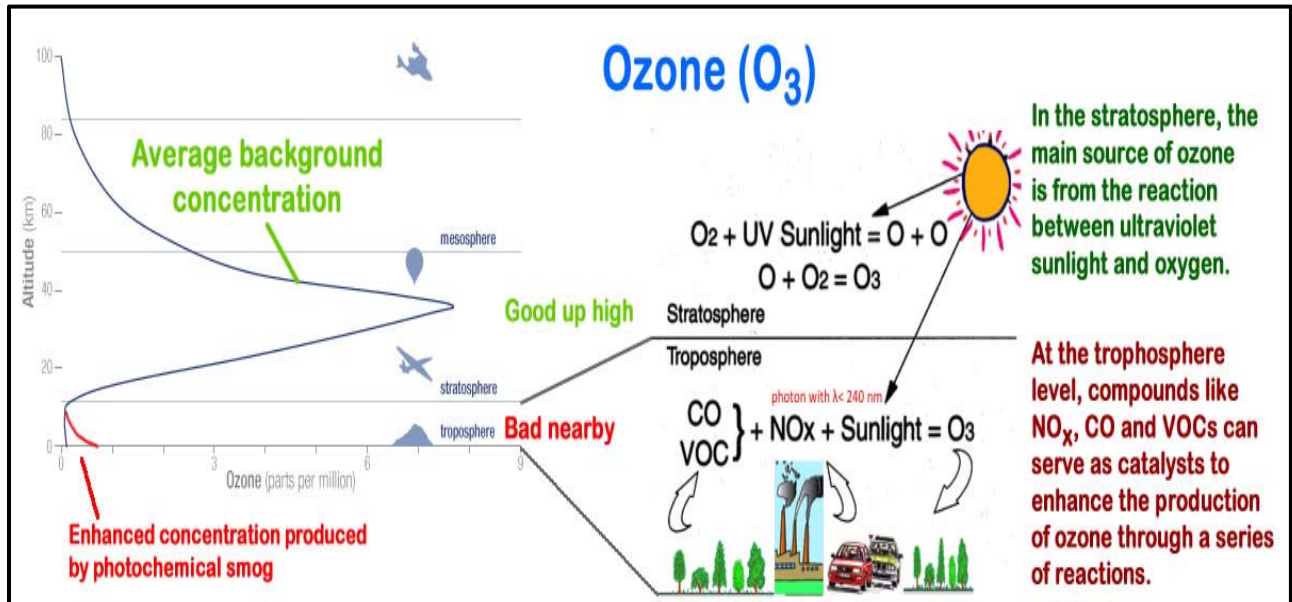


Fig. 2 (b) Good and bad ozone

Courtesy: [http://tecalive.mtu.edu/envengtext/ch12\\_criteria.htm](http://tecalive.mtu.edu/envengtext/ch12_criteria.htm)

Pollutant gases, particularly, reactive halogen gases (Fig. 2 (c)) such as chlorine and bromine compounds in the atmosphere are responsible to cause the ozone depletion, which is mainly observed in the 'ozone hole' over Antarctica and over the North Pole. Most of the chlorine, and nearly half of the bromine in the stratosphere, where most of the depletion has been observed, comes from human activities.

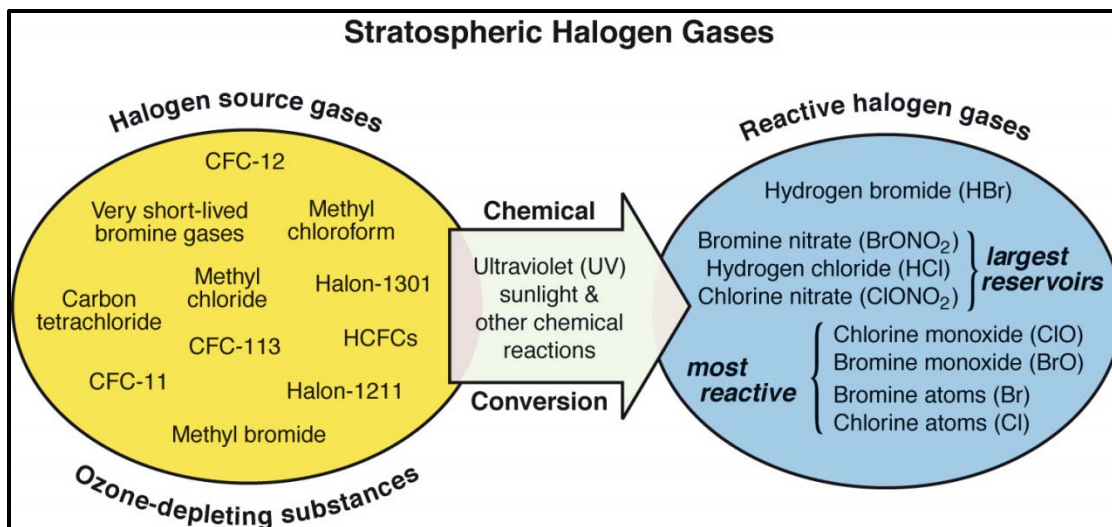


Fig.2 (c) Halogen gases

Courtesy: <http://eschooltoday.com/ozone-depletion/what-is-ozone-depletion.html>

Fig. 2 (d) shows a schematic illustrating the life cycle of the chlorofluorocarbons (CFCs); how they are transported up into the upper stratosphere/lower mesosphere, how sunlight breaks down the compounds and then how their breakdown products descend into the polar vortex.

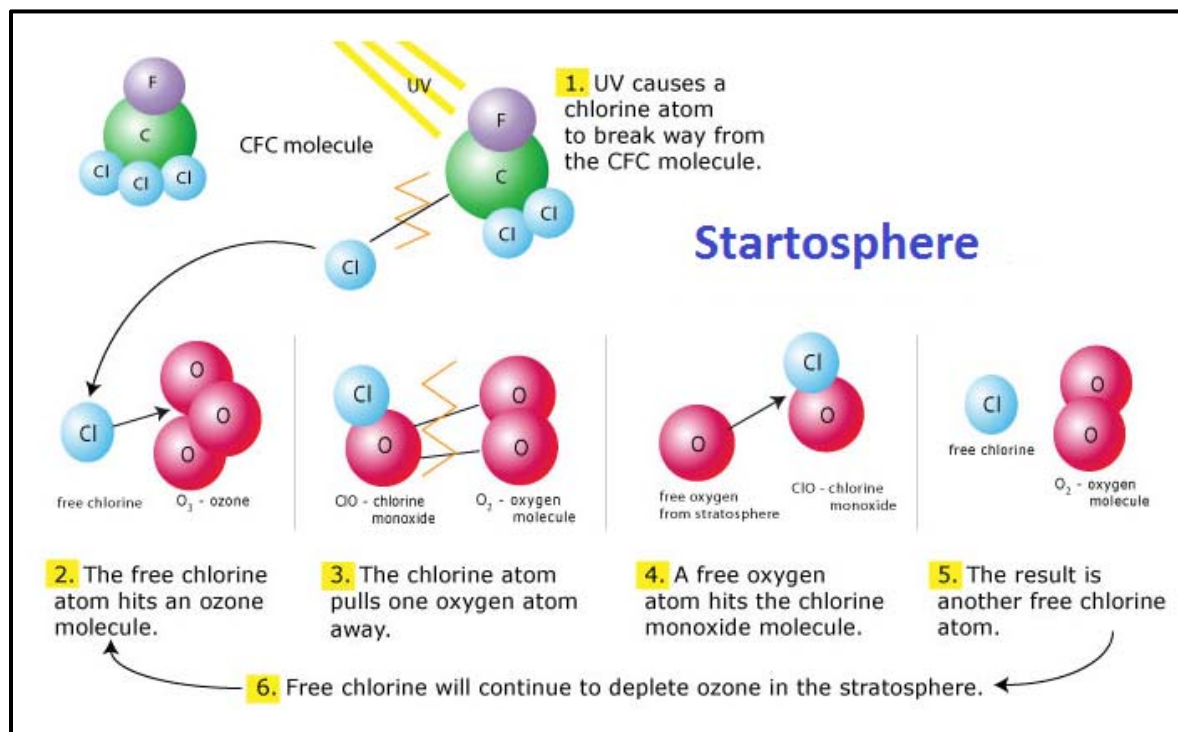


Fig. 2 (d) Chemical processes of ozone depletion and CFCs  
<http://www.esu.edu/~scady/parise/3reactions.htm>

HASP-NASA provided a platform for 12 small payloads and 4 large payloads. The maximum mass limit was 20 kg for a large payload and 3 kg for a small payload. UND and UNF jointly had one small payload. UNF team fabricated the gas sensors system, payload body, microcontroller circuit, software, and electronic communication circuits. The HASP had an onboard computer, power supply batteries, GPS, video camera, and communication link for all payloads. UNF team participated in the workshop at the NASA-Columbia Scientific Balloon Facility (CSBF) in Palestine, Texas during July 27 to August 1, 2014 for the integration of the sensors payload with the HASP. Ozone sensor payload was then integrated with the HASP platform. The UND-UNF payload successfully passed all required thermal vacuum tests and certified for the flight. Then, the HASP2014 flight was launched successfully by NASA-CSBF on August 9, 2014 from Fort Sumner, New Mexico. The flight duration was short and about half to that of previous year's flights. During the flight, the UNF ozone sensors array worked and detected ozone in the stratosphere. The payload sent out the data files during the flight without any problem. After the termination of the balloon flight, the payload landed safely on the ground using a parachute. Then, the payload was recovered. The technical details, pictures and science results of this flight are highlighted in this report.

## 2. Fabrication of Nanocrystalline Thin Film Gas Sensors

Ozone sensors were fabricated by UNF team at Dr. Patel's sensors laboratory at the UNF. Fig.3 show (a) and (b) shows thermal vacuum deposition system and electron beam deposition system, respectively, were used to fabricate nanocrystalline nanocomposite thin film gas sensors for the detection of ozone gas.



Fig. 3 (a) Thermal vacuum deposition system and (b) electron beam deposition system

Fig. 4(a) shows the top view of one typical low magnification scanning electron microscope image of the Indium Tin Oxide (ITO) thin film gas sensor having two gold electrodes for external electrical contacts.

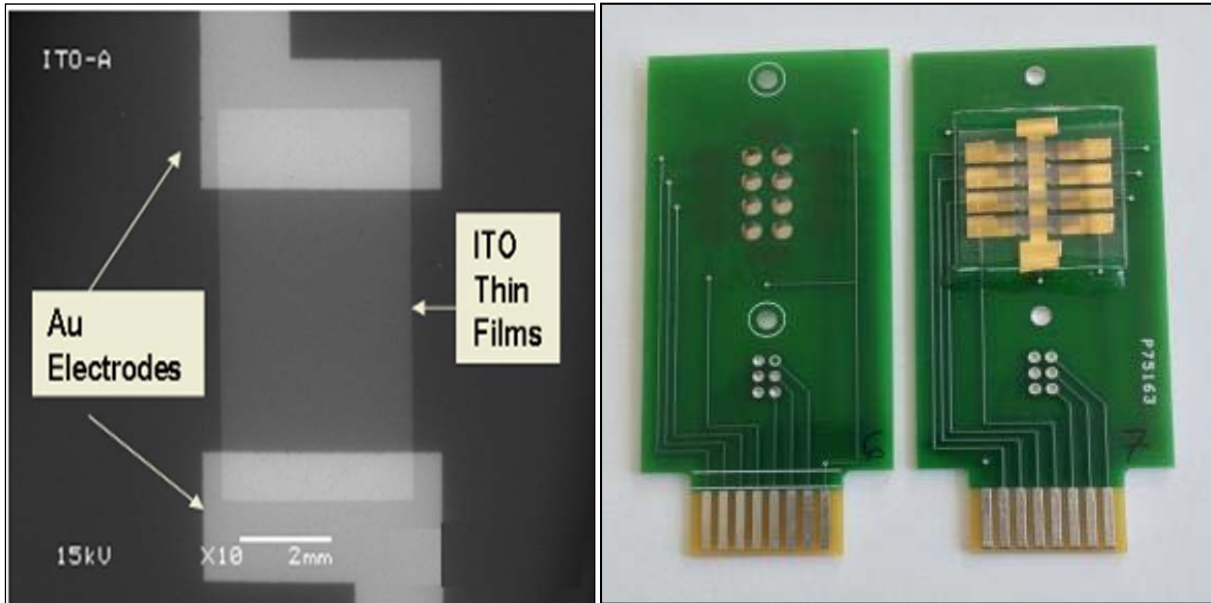


Fig.4 (a) Scanning electron microscope image of top view of one ITO thin film gas sensor (size: 2 x2 mm), (b) Top and bottom view of 8 gas sensor array interface with the printed circuit board (size: 4 x 7 cm) (UNF Patent pending)

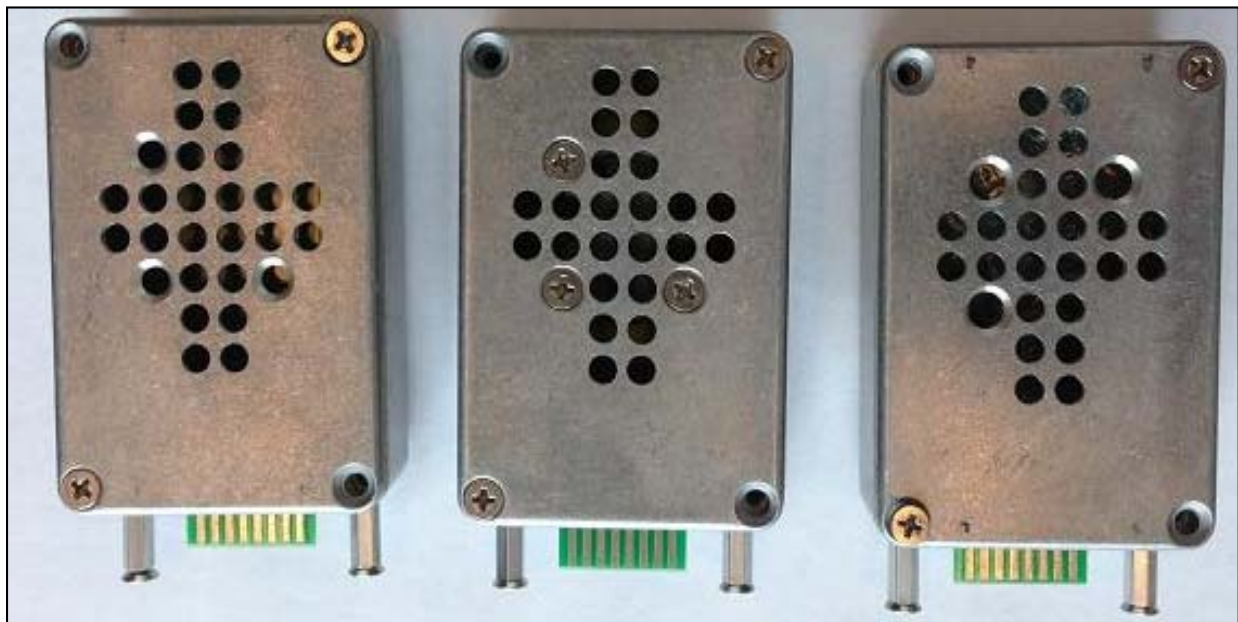


Fig. 4(c) Three sensors boxes # 1, 3 and 4 (size 5.5 x 2.5 x 8.0 cm)

Fig. 4 (b) shows a typical array of 8 ITO thin film gas sensors fabricated on an approximately 2.5cm x 2.5cm ultra cleaned glass slide. The glass slides were throughlly cleaned by the ultrasonic cleaner, detergent, solvant and baked in the ovan. The interface of the cicuit board to the array is also shown in. Fig. 4(b). Three types of sensor array boxes were fabricated as shown in Fig. 4(c). Each type of sensor array was mounted in a separate box. In addition to the sensors box for the payload, three backup sensors PCB boxes were fabricated. All sensors boxes were calibrated at UNF by UNF students team members (Brittany and Ken) at different time period and then tested in the thermal vacuum test chamber at CSBF, Palestine, TX.

**Box #1** sensors are nanocrystalline ITO thin film deposited on glass for detection of ozone.

**Box #3** sensors are ZnO + ITO thin films deposited on glass for detection of ozone.

**Box #4** sensors are nanocomposite of WO<sub>3</sub> + ITO thin films deposited on glass for detection of reducing gas.

**Backup Box# 6, 5 and 2.**

Fig. 5 (a) shows the picture of housing for the UNF sensors, consisting of an array of 8 gas sensors interfaced with a printed circuit board (PCB), flexible Kapton heater (MINCO make HK 5573R30.0 L12BU), temperature sensor ( Analog Device TMP36), electrical fan (SUNON, MC25060V2-0000-A99, DC 5V, 0.38W) and a 16 wires flat cable. One end of flat cable has a female card edge connector to connect sensor PCB (Make: 3M, MCS16K-ND), while other end has 16 pin female to connect microcontroller PCB.

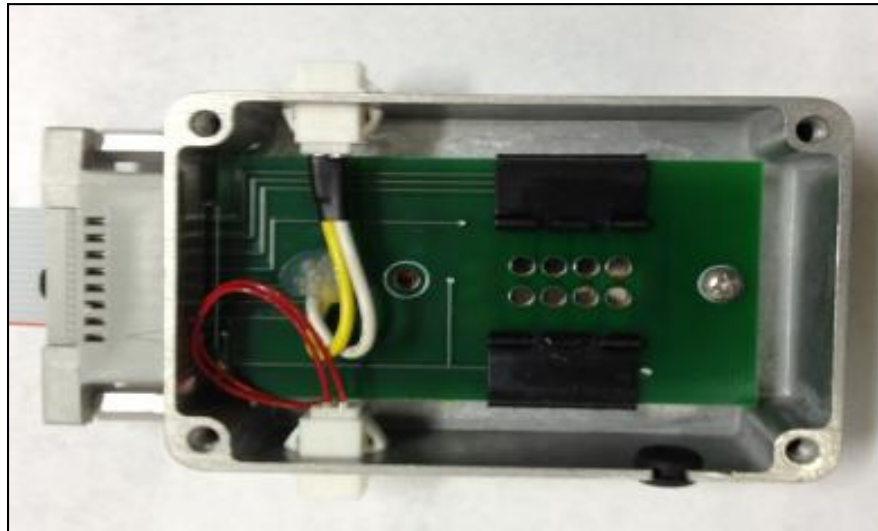


Fig.5 (a) Inner view of UNF Ozone sensors box

The pin information of sensor PCB and connector are shown in fig. 5(b) and (c), respectively.

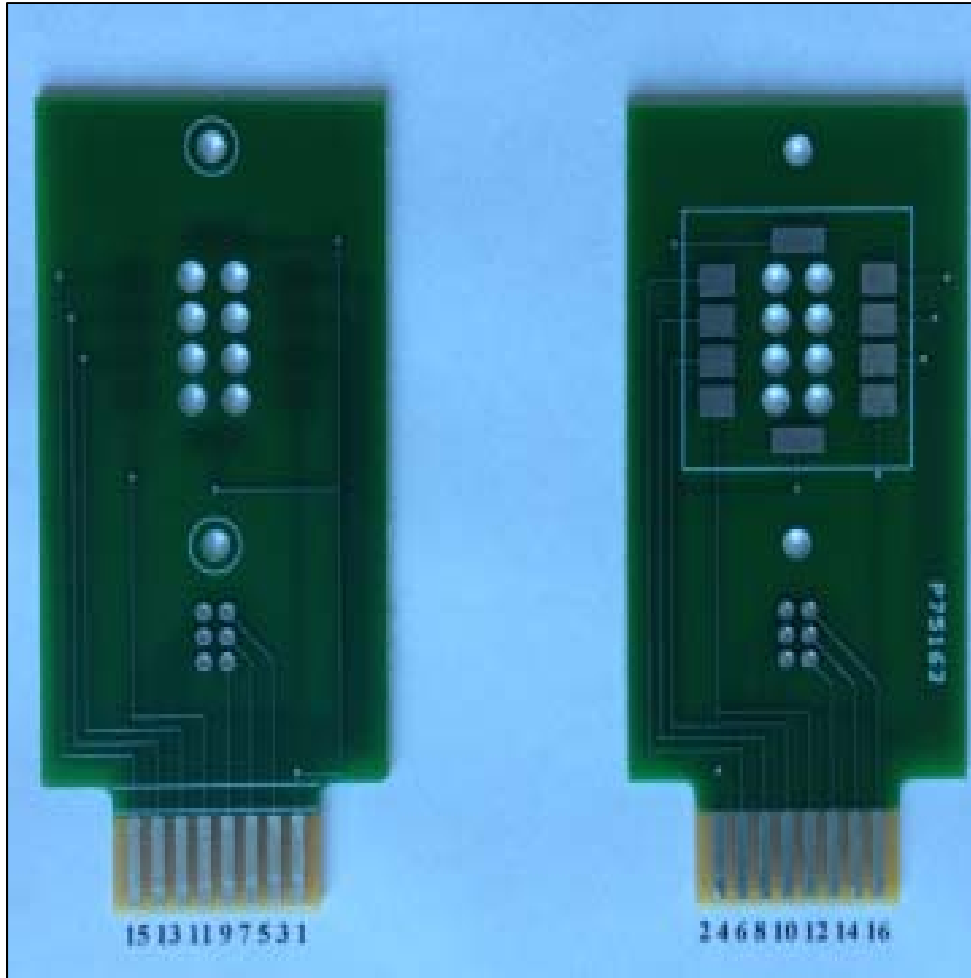


Fig.5 (b) Pin numbers of sensors PCB

Pin number per connector datasheet							
1	3	5	7	9	11	13	15
Common	Temp Sensor	Temp Sensor	Temp Sensor	Gas Sensor	Gas Sensor	Gas Sensor	Gas Sensor
Open	Gas Sensor	Gas Sensor	Gas Sensor	Gas Sensor	Light Sensor	Light Sensor	Pin not used
2	4	6	8	10	12	14	16
Pin number per connector datasheet							

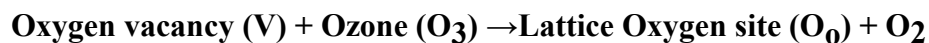
Fig.5 (c) Pin information for connection of 16 pins female card edge connector with sensors PCB

### 3. Working Principles of Gas Sensors

#### Interaction of oxidizing gas on surface of n-type ITO thin film sensor

Upon adsorption of charge accepting molecules at the vacancy sites, namely from oxidizing gases such as ozone (O<sub>3</sub>), these electrons are effectively depleted from the conduction band of ITO. This leads to an increase in the electrical resistance of n-type ITO.

*For ozone gas:*

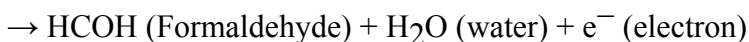
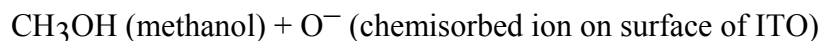


Vacancies can be filled by the reaction with ozone. Filled vacancies are effectively electron traps and as a consequence the resistance of the sensor increases upon reaction with ozone.

#### Interaction of reducing gas on surface of n-type ITO thin film sensor

Oxygen vacancies on ITO surfaces are electrically and chemically active. These vacancies function as n-type donors decreasing the electrical resistivity of ITO. Reducing gases such as CO, H<sub>2</sub> and alcohol vapors result in detectable decreases in the electrical resistance of n-type ITO.

*For methanol:*



Vapors come in contact with the surface and react with chemisorbed oxygen ions O<sup>-</sup> or O<sup>2-</sup> and re-inject electrons into the conduction band.

In summary, the electrical resistance of ITO increases in the presence of oxidizing gases such as ozone. Upon adsorption of the charge accepting molecules at the vacancy sites, namely oxidizing gases such as ozone, electrons are effectively depleted from the conduction band, leading to an increase in the electrical resistance of n-type ITO. Note that our three different types of sensors boxes have n-type semiconductor gas sensors.

## 4. Calibration of Gas Sensors

The ITO sensors array was first tested and calibrated in the test chamber at UNF. The test chamber was adjusted to the identical conditions of temperature and pressure as in the stratosphere. Fig. 6(a) and (b) shows the pictures of ozone generator and detector used for the calibration of sensors. An ozone generator (Ozone Solutions, Model# OMZ-3400) was used as the source of ozone, which generated 0 to 12 ppm ozone gas.

A digital ozone detector (Eco Sensors, Inc., Model:A-21ZX) was used to measure the concentration of ozone in part per million (ppm). The Keithley digital multimeters and electrometers attached with computer having LabView program were used for the measurements of the ITO sensor's resistance.

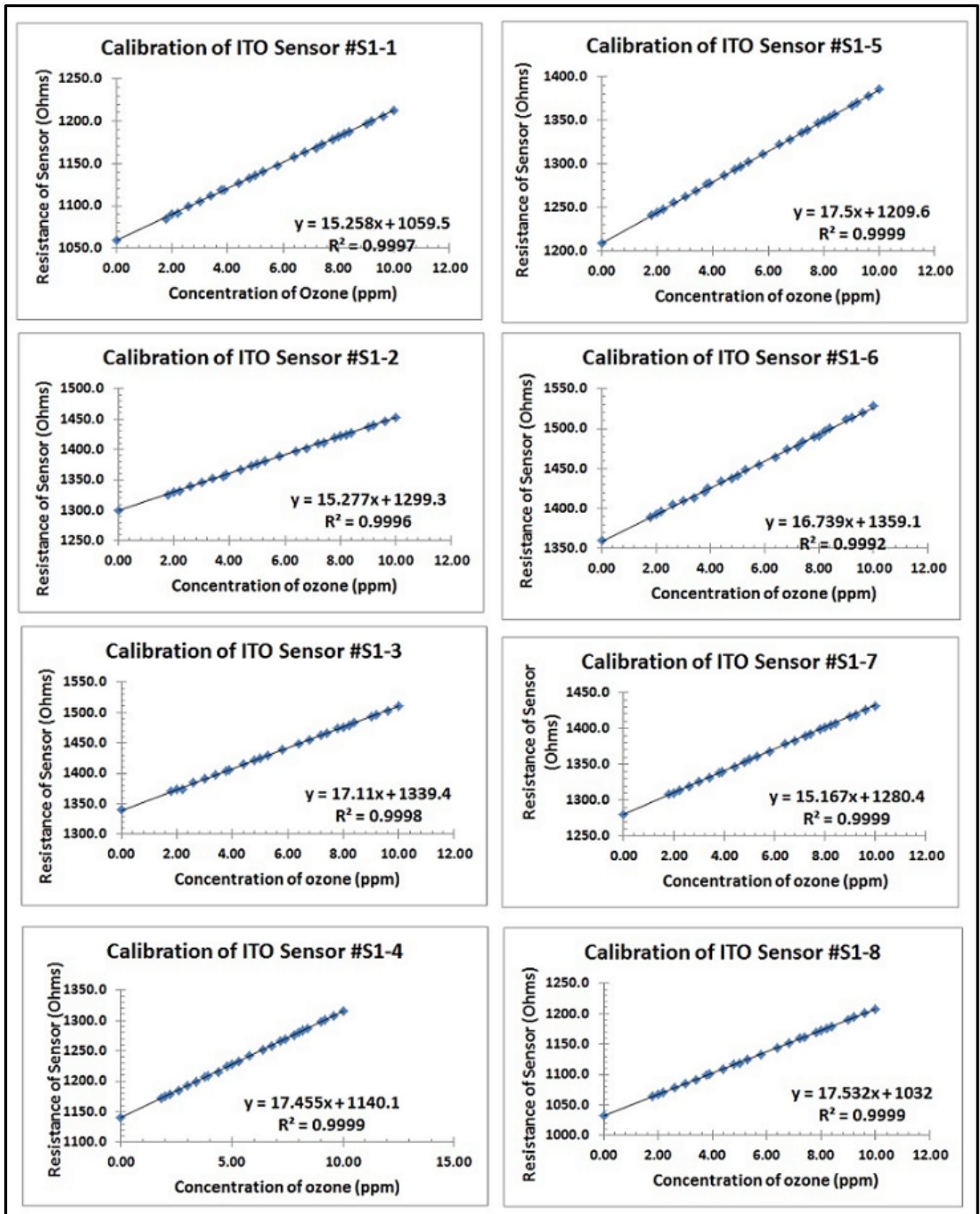


Fig.6(a) Ozone generator and (b) digital ozone detector

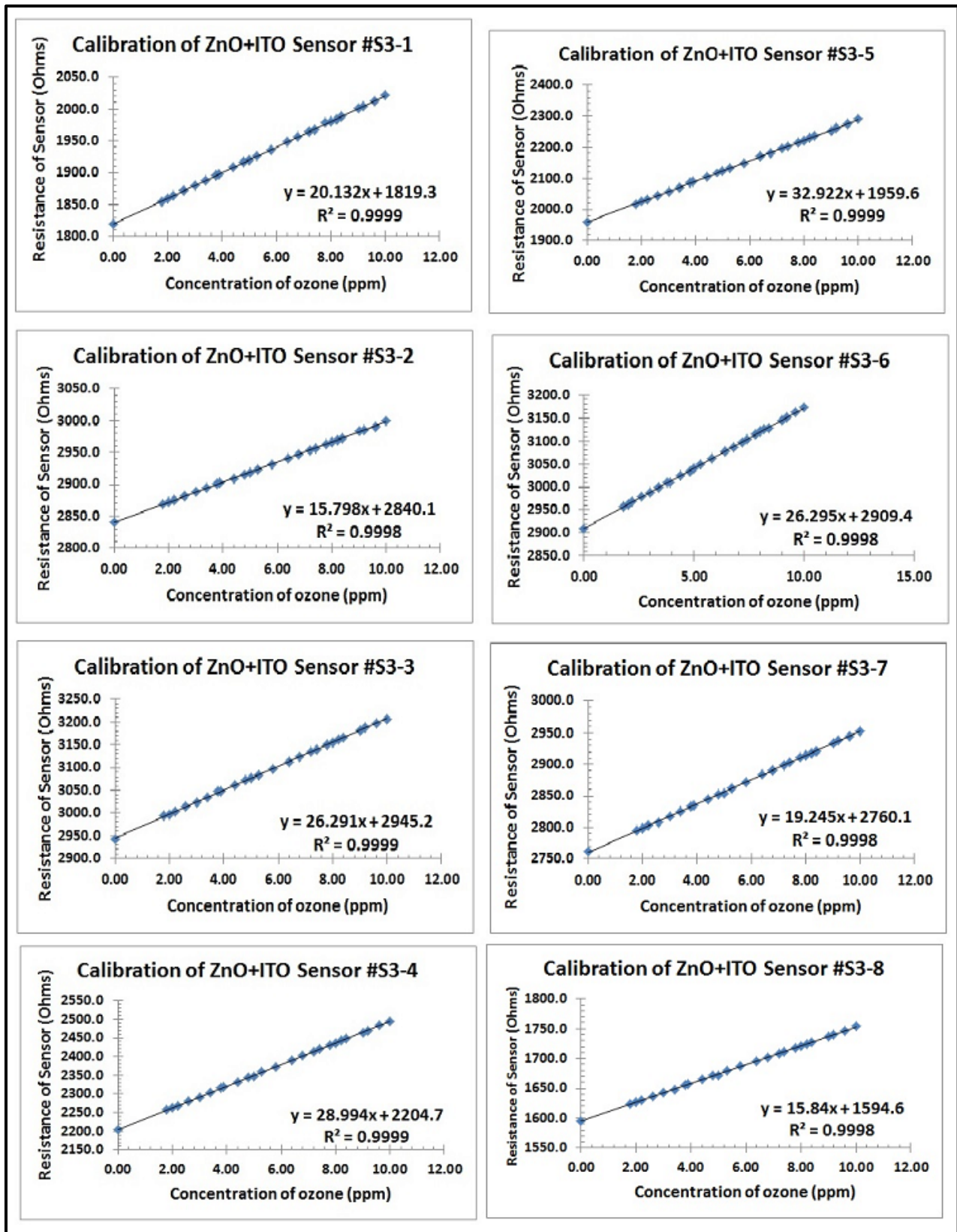
All the 24 sensors of sensors box was calibrated simultaneously under identical conditions of pressure, temperature and concentration of ozone in the test chamber. The sensors were calibrated with ozone gas in the range of 0.02 to about 10.00 ppm in the test chamber in the same run. The usual variation of ozone in the stratosphere is about 3.0 to 10.0 ppm. The measured data fit linearly and trend line equations for each plot were determined.

Figs.7 (a) show the calibration plots ozone sensors Box#1 having sensors # S1-1 to S1-8. These sensors were made of nanocrystalline ITO thin film gas sensors fabricated on the glass.

Figs.7 (b) show the calibration plots ozone sensors Box#3 having sensors # S3-1 to S3-8. These sensors were made of nanocomposite of ZnO + ITO thin film and were fabricated on the glass.



Figs.7 (a) show the calibration plots ozone sensors Box#1 having sensors # S1-1 to S1-8.



Figs.7 (b) show the calibration plots ozone sensors Box#2 having sensors # S3-1 to S3-8.

The calibration plots ozone sensors Box#4 having sensors # S4-1 to S4-8 were also performed with few reducing gases. The plots are not presented here. These sensors were made of nanocomposite of  $WO_3$  and ITO thin film gas sensors fabricated on the glass. All sensors were calibrated at three different times and showed nearly the same nature of response each time. Small variations in the slope and y-intercept values were observed due to the variation of sensor thickness and experimental error.

## 5. Fabrication of Payload Body

The main features of our newly designed payload body are easy to open and close payload, easy access of PCB and sensor boxes, low rate of outgassing under low pressure, better stability with thermal and impact, and reusable. The following parts were procured for payload body from supplier [www.onlinemetals.com](http://www.onlinemetals.com).

Name	Size	Purpose
Aluminum Extruded Square Tube  Part #6063-T52	height 11"  w x d: 6" x6"  wall thickness: 0.125"	Payload body
Aluminum Sheet  Part#3003-H14	6" X 6"  Thickness:1/8"	Top lid
Aluminum Finished Rectangles  Part#2024-T351	0.625"X1"	Internal support of payload with base plate and lid

Ken Emanuel made design and fabricated payload body in the workshop of Department of Engineering of UNF. Design diagrams are shown in Fig. 8 (a) to (k).

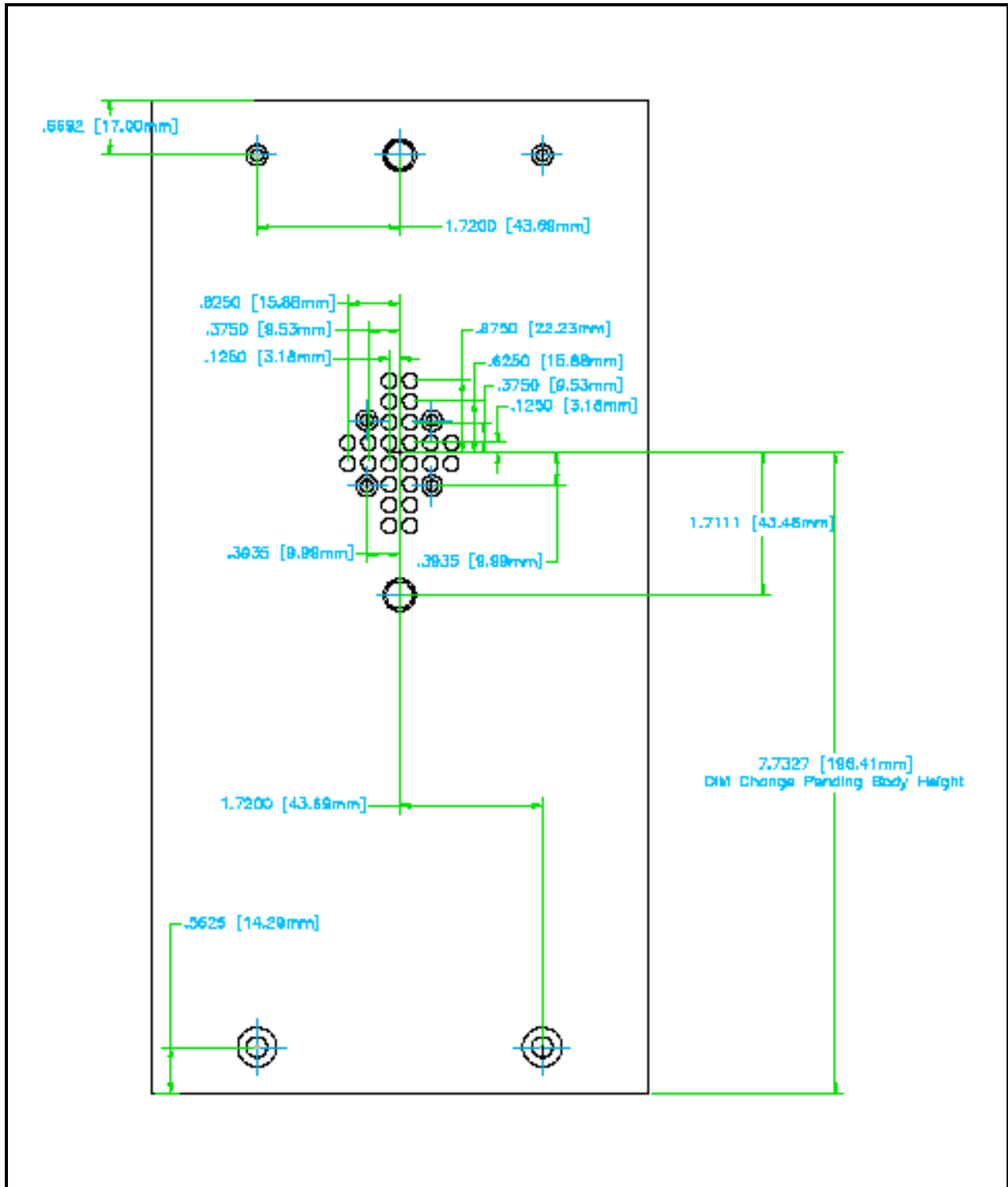


Fig.8 (a) Design for holes on two opposite sides (Side #1 and 3) of payload body

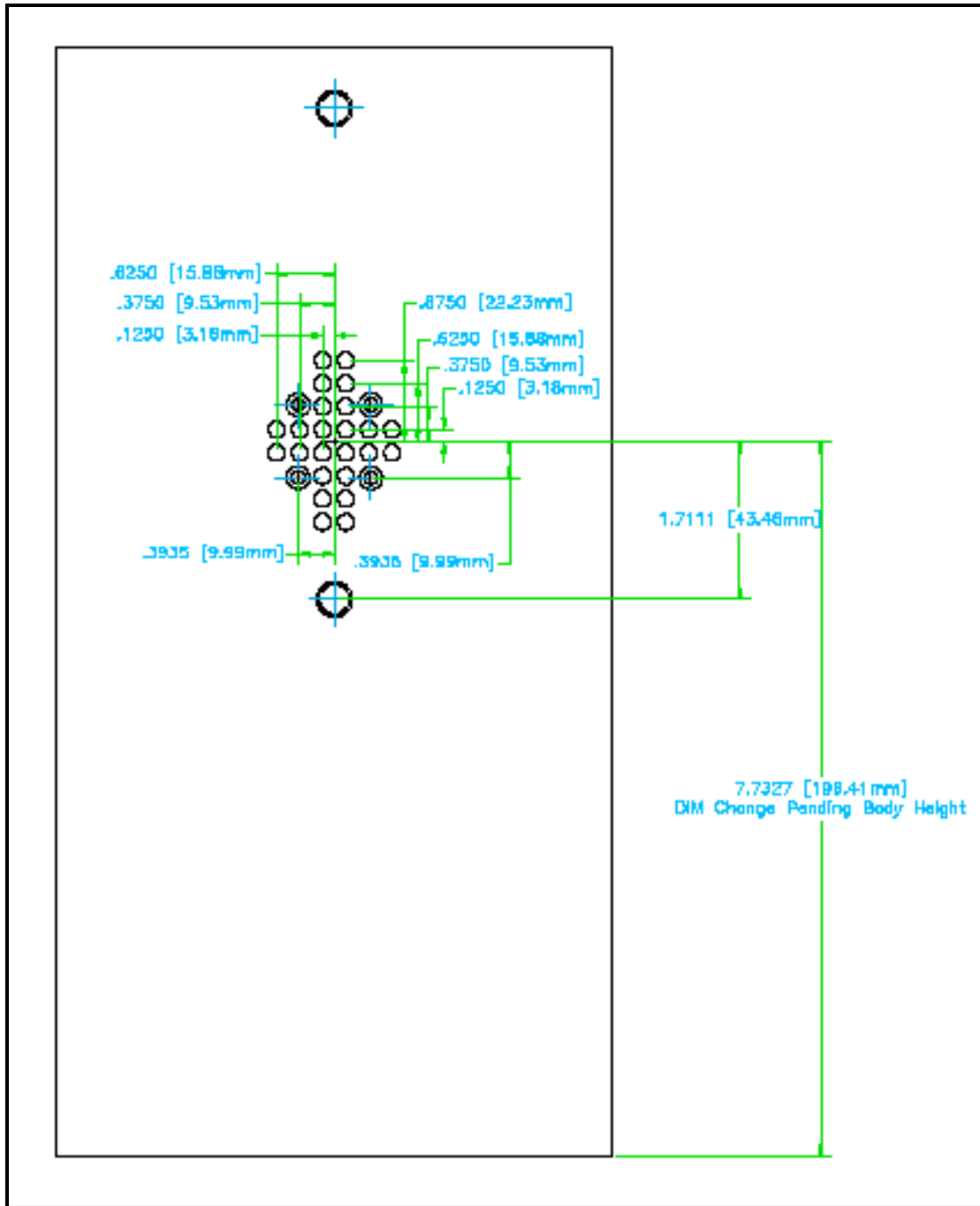


Fig 8 (b) Design for holes on Side # 2 of payload body

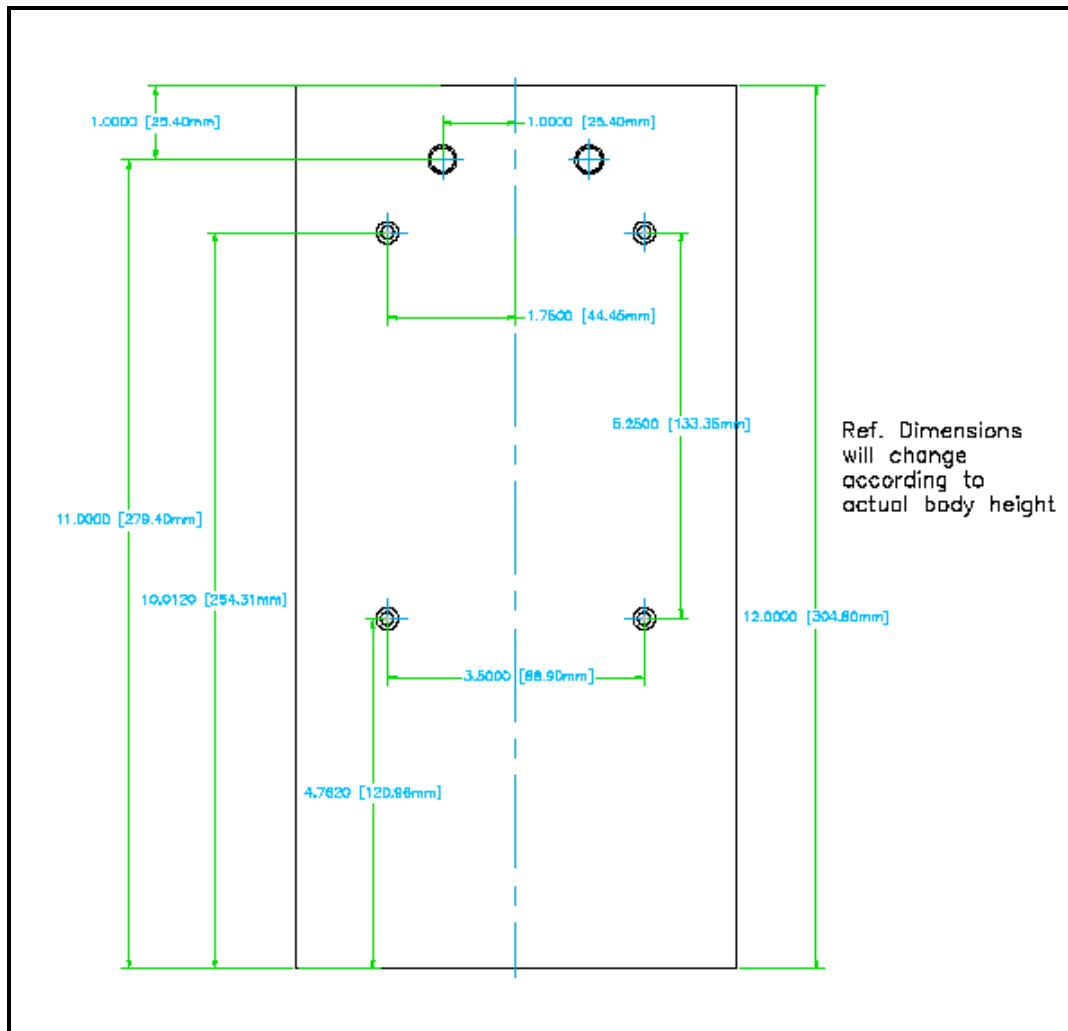


Fig.8 (c) Design for holes on fourth side (Side #4) of payload body for mounting microcontroller PCB

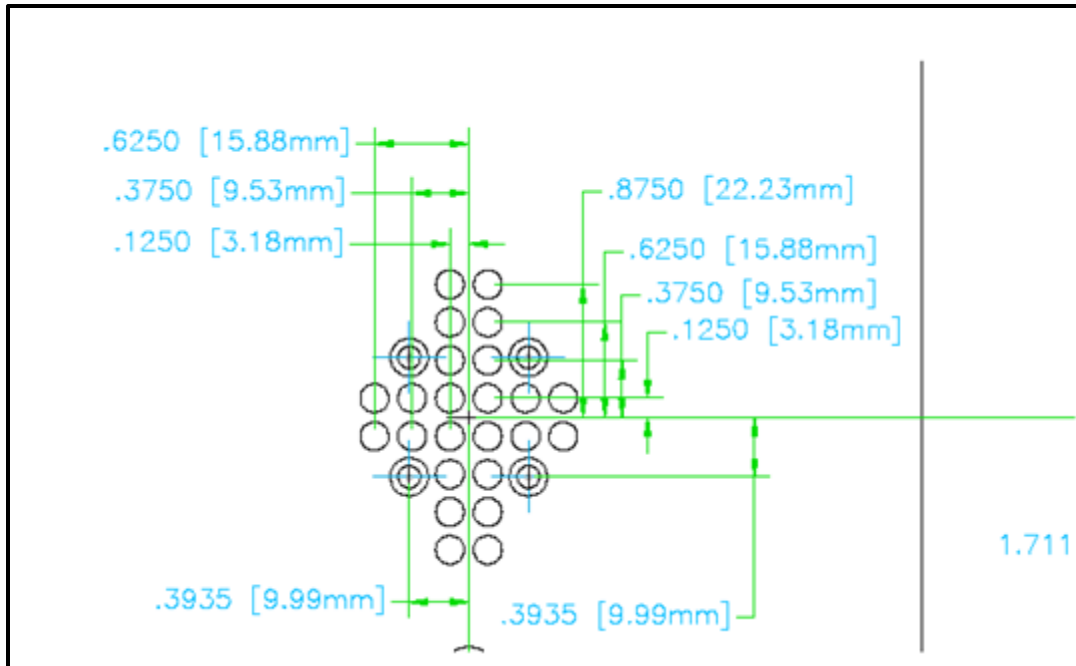


Fig.8 (d) Details of design for holes on three sides of payload body for fan and air inlet

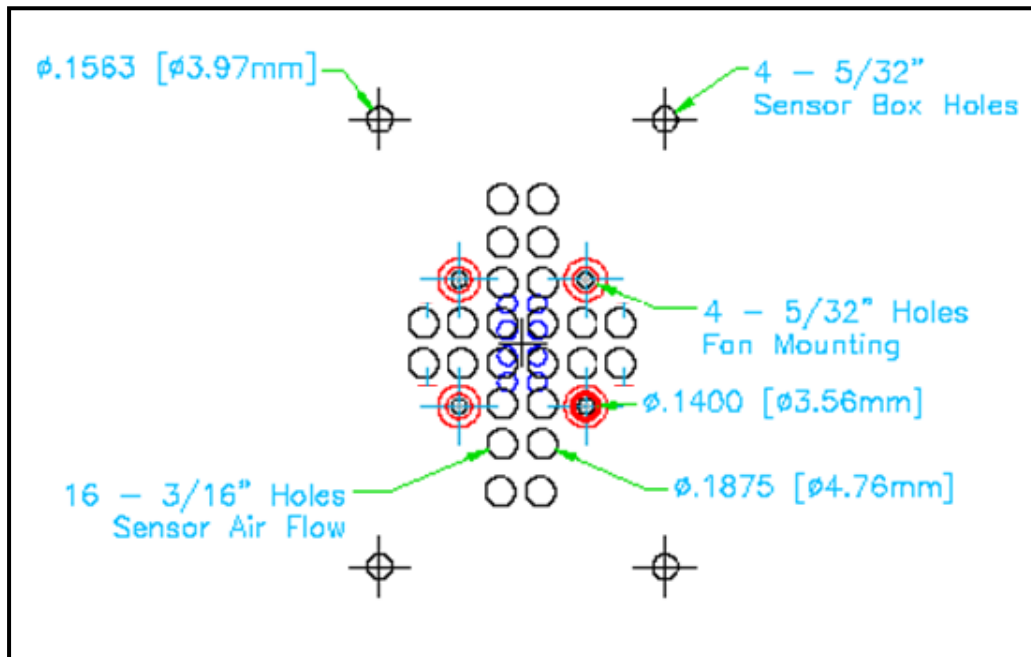


Fig.8 (e) Details of design for holes on three sides of payload body and sensor box

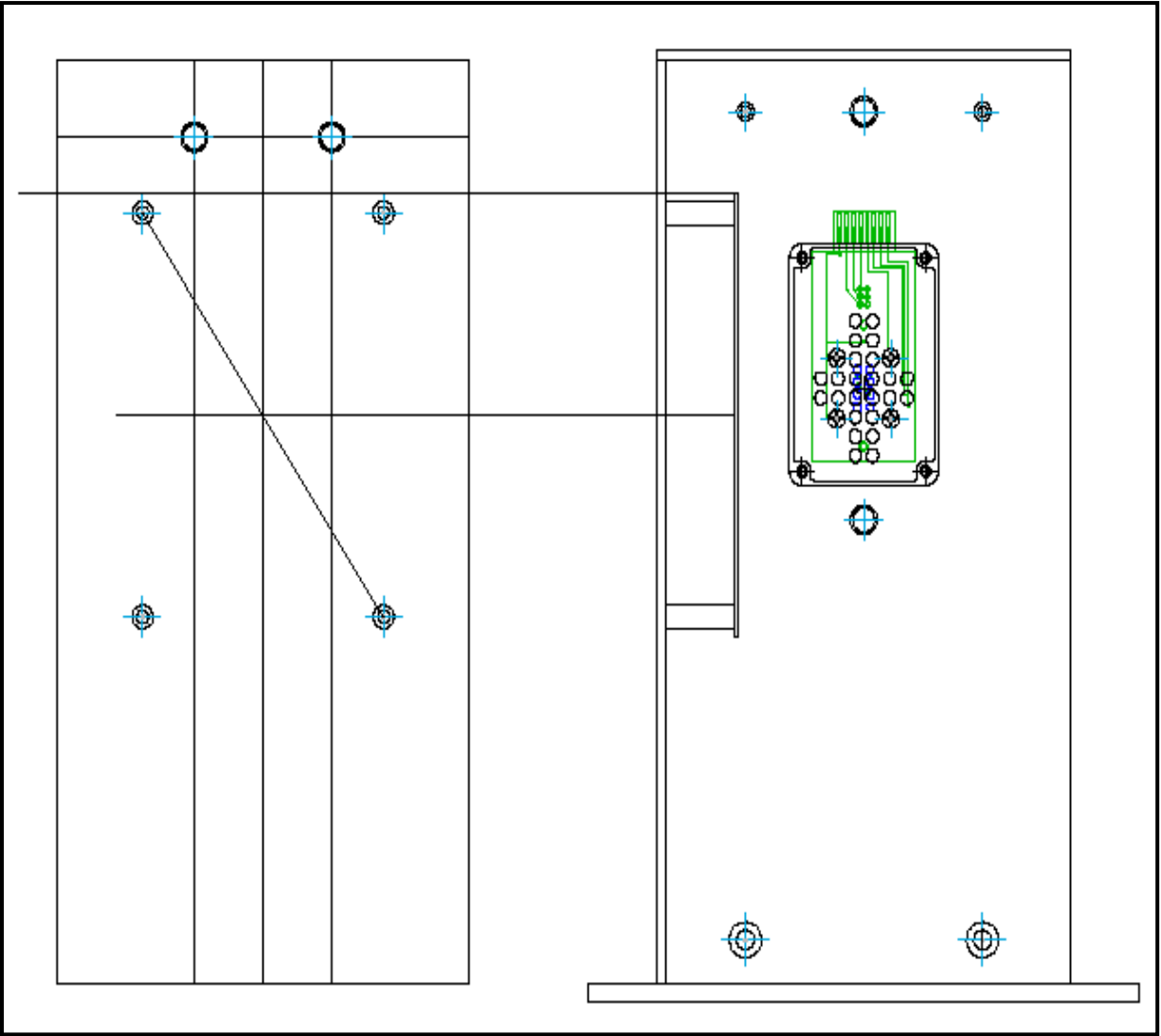


Fig.8 (f) Design for holes on payload body for mounting microcontroller PCB and sensor box

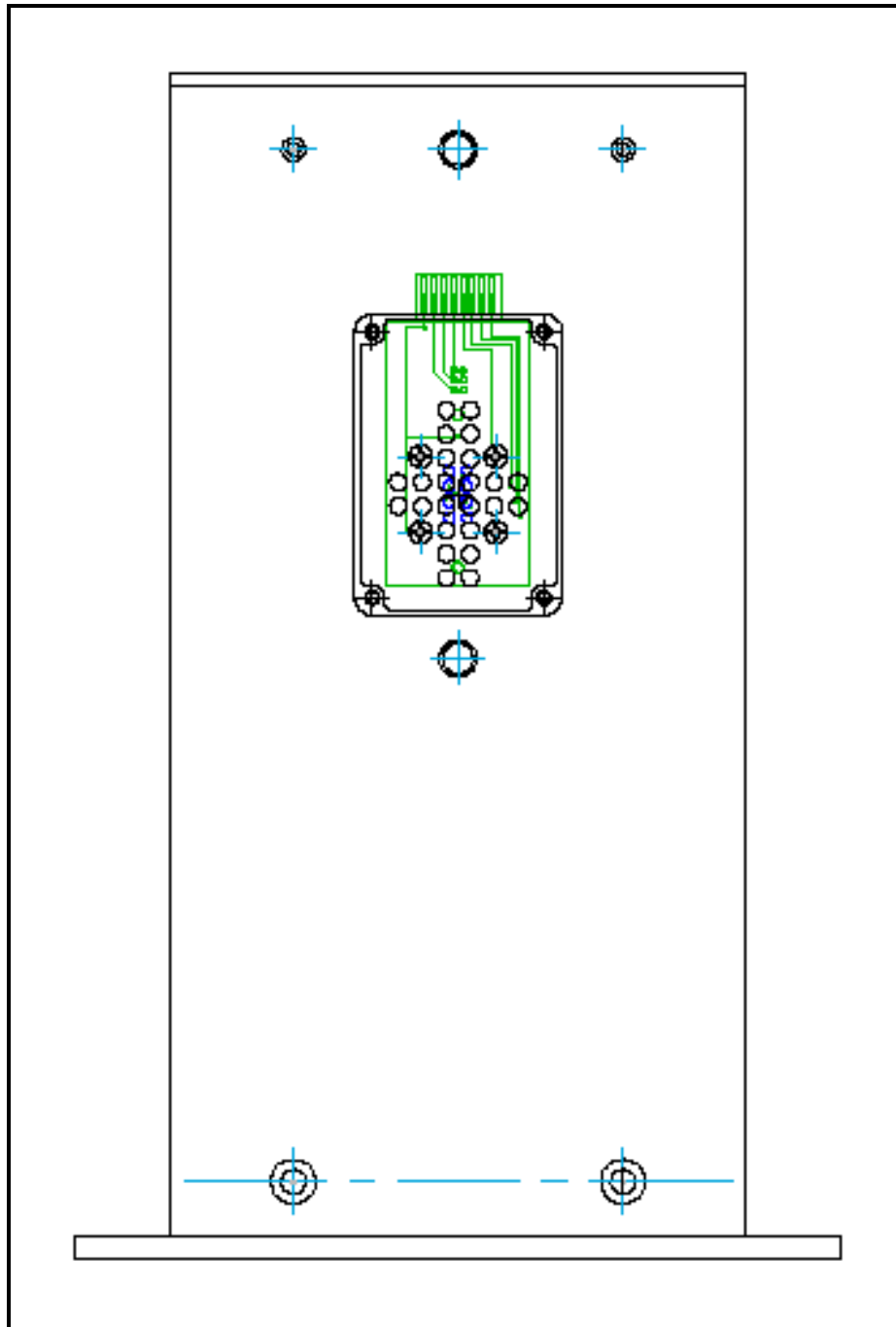


Fig.8 (g) Design for holes on payload body for mounting of sensor box, LED, Light sensor and HASP mounting plate

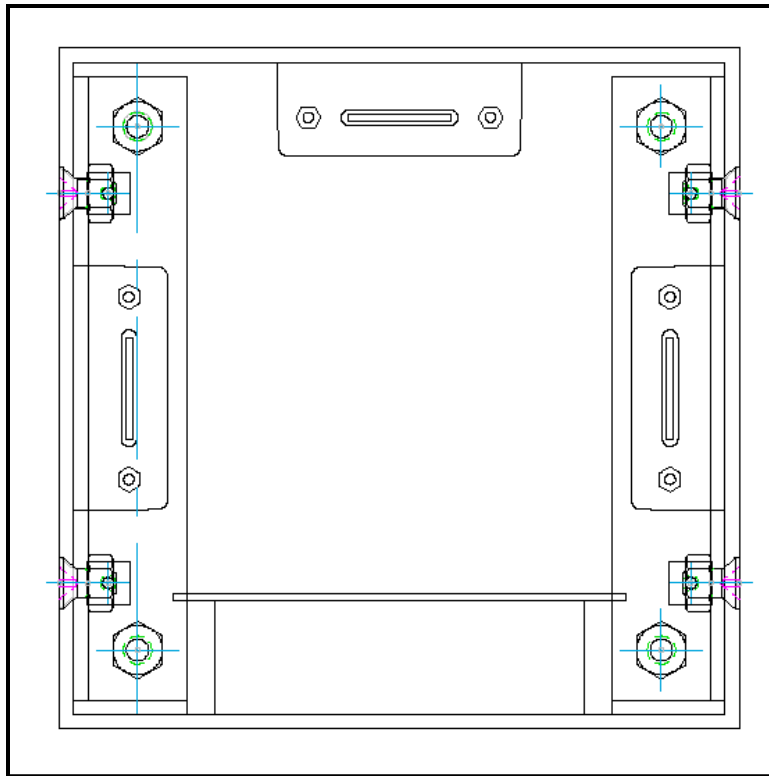


Fig.8 (h) Top view of payload

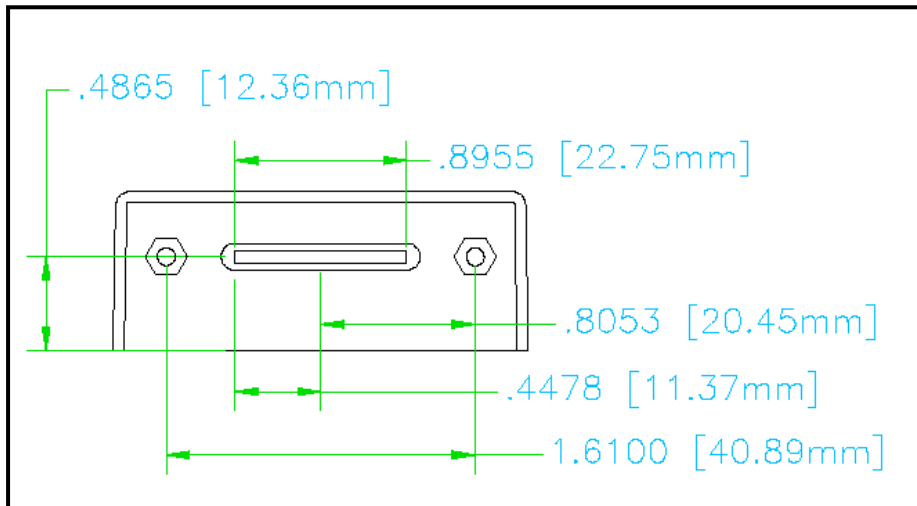


Fig.8 (i) Design for standoff and PCB slot in the sensor box

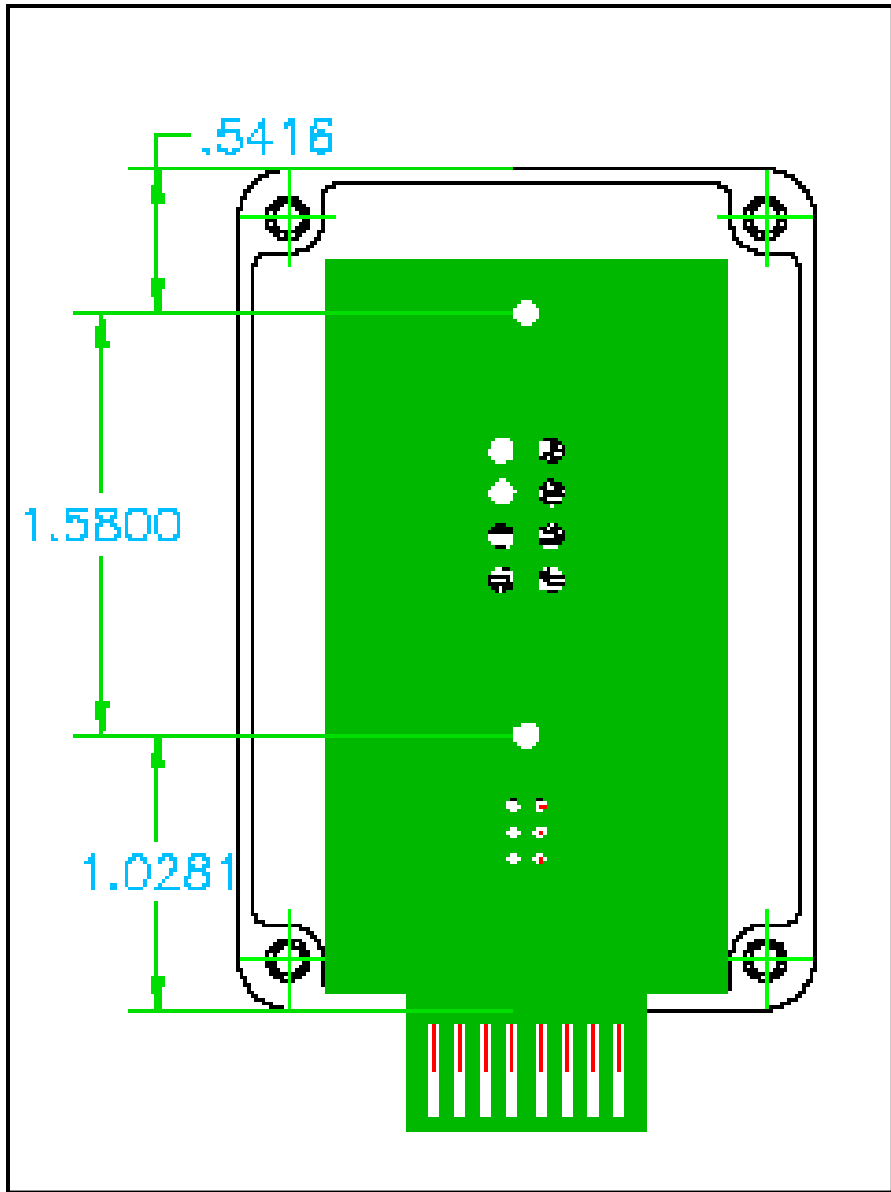


Fig.8 (j) Design for standoff to mount sensor SPCB in the box

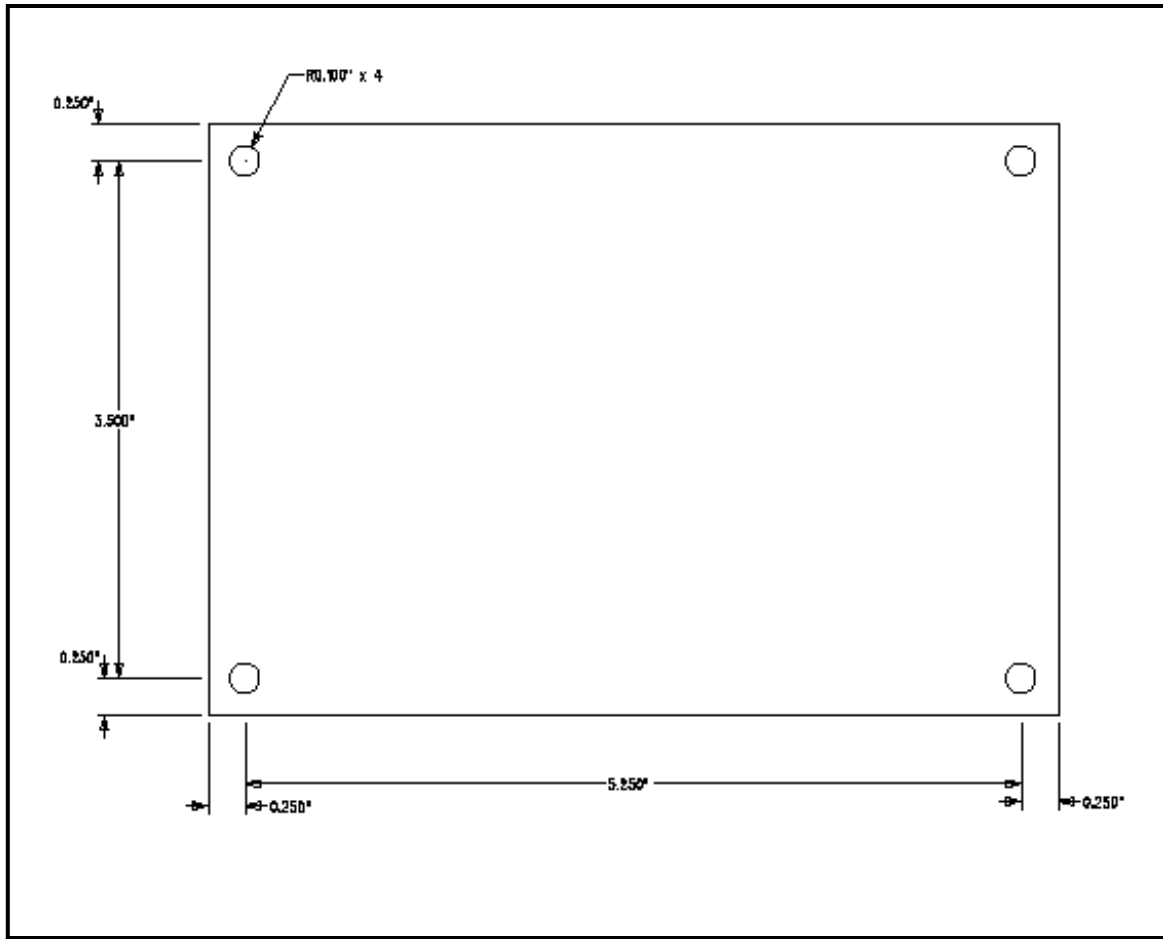


Fig.8

(k) Design for hole of the microcontroller PCB

The pictures of the payload body are shown in fig.8 (l) to (n). The dimensions of payload were 296mm x 149mm x 149mm, which were within the requirement of being less than 300mm x 150mm x 150mm.



Fig.8 (l) Ken (UNF) fabricating the payload body using CNC machine (Micromill 2000)

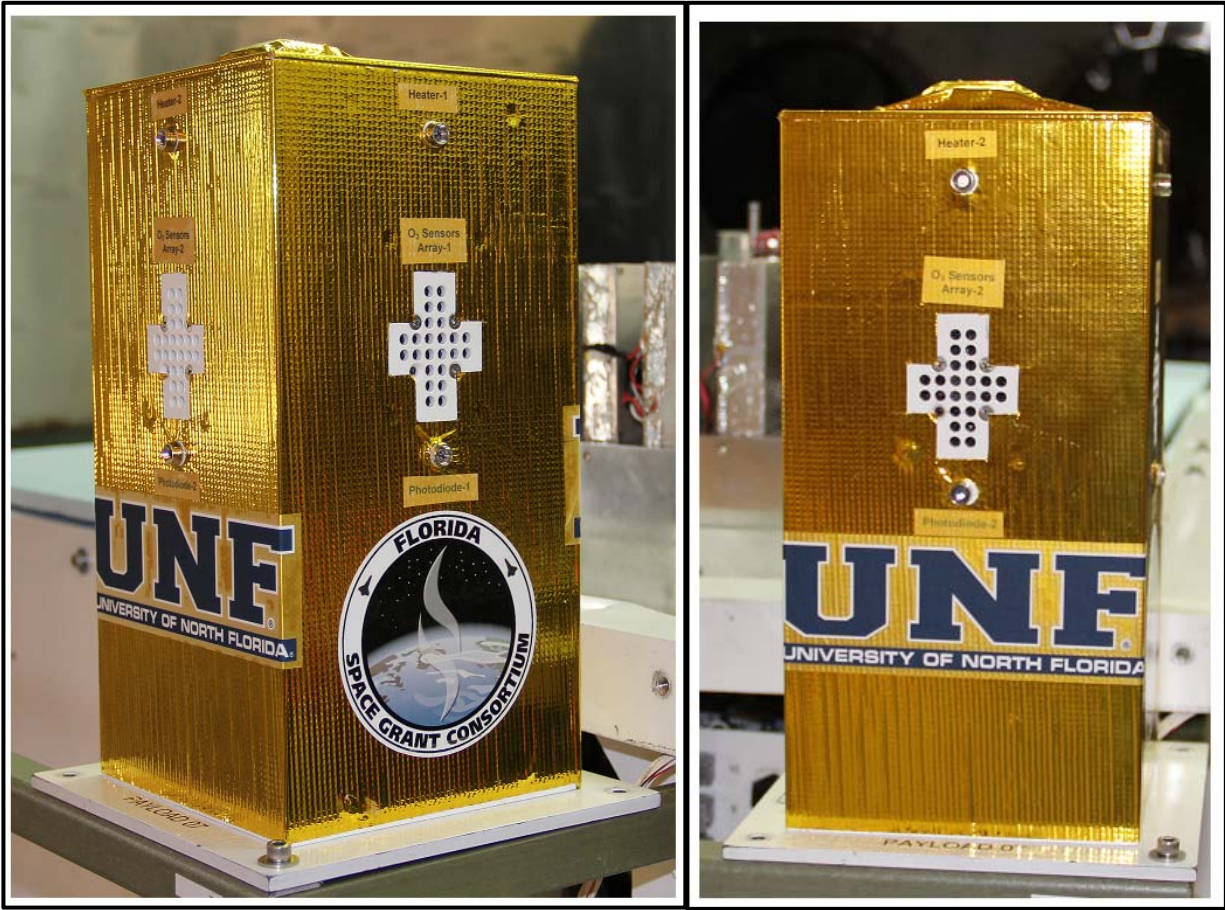


Fig.8 (m) and (n) Payload body structure

Item	Dimension	Mass (g)
8 Ozone sensors box #1 (including fan, heater, box)	3 x 2 x 1 inch	200.00 g
8 Ozone sensors box #2 (including fan, heater, box)	3 x 2 x 1 inch	200.00 g
8 Pollutant sensors box#3 (including fan, heater, box)	3 x 2 x 1 inch	200.00 g
Microcontroller PCB with mounted components	4 x 6 inch	300.00 g
Payload body, top plate and thermal blanket	11 x 6 x 6 inch	1295.00 g
Few Cables, 1 GPS, 2 LEDs, 3 Photodiodes, nuts and bolts		450.00 g
HASP mounting plate	7.9 x 7.9 inch	560.00 g
<b>Total</b>		<b>3205.00 g</b>

Fig.9 Weight budget of various parts of the payload

Fig.9 shows weight budget of various parts of the payload. The final total mass of payload including its base plate was 3.20 kg, which was less than the limit of 3.00 kg + 0.50 kg mass of base plate (total 3.5 kg).

## 6. Electronic Circuits

The block diagram of circuit is shown in fig. 10 (a), while several sections of circuits are shown in fig. 10 (b) to (h). Two identical microcontroller PCBs were fabricated. The picture of PCB is shown in fig.10 (i). Two identical PCBs were fabricated. One PCB was used for the payload, while for other PCB was used to stimulate software and backup. The microcontroller circuit was developed by Jonathan Wade (UND) earlier.

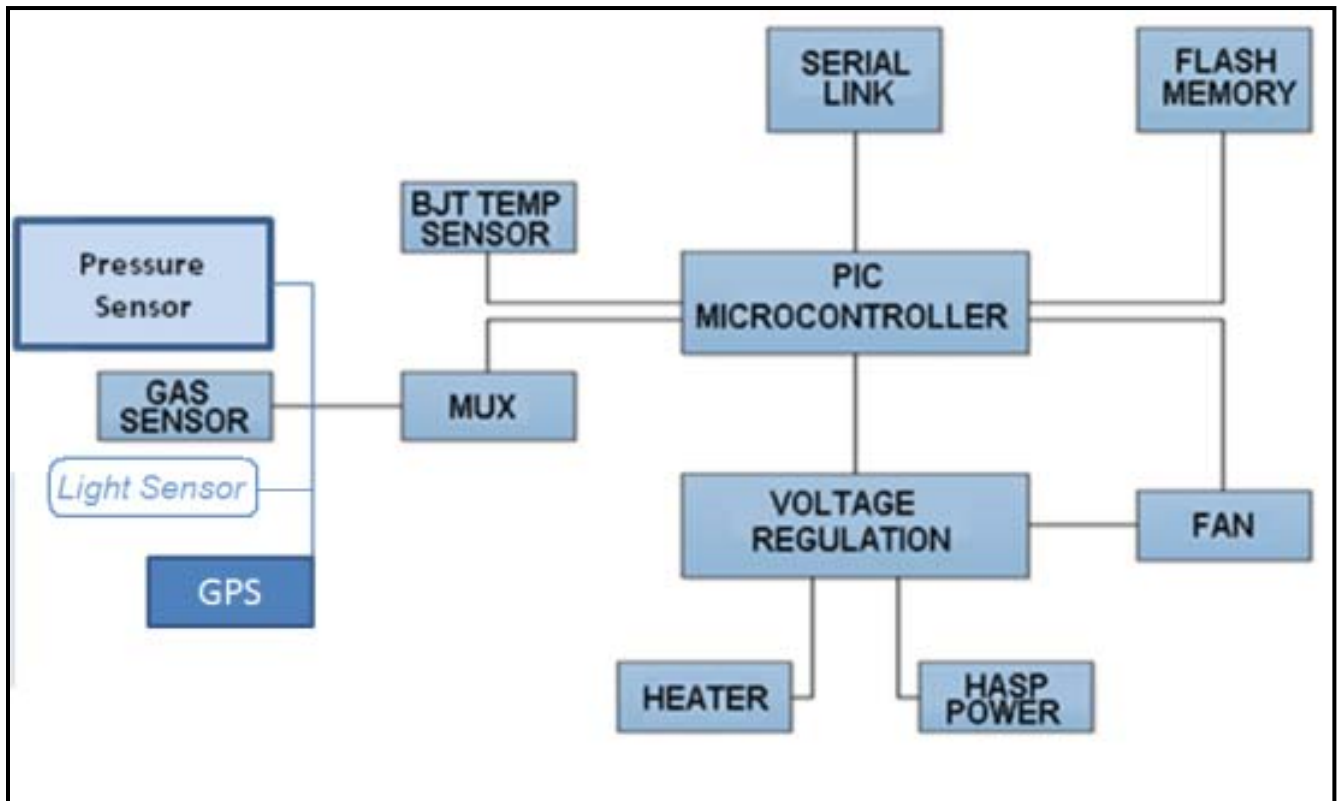


Fig. 10(a) Block diagram of payload circuit



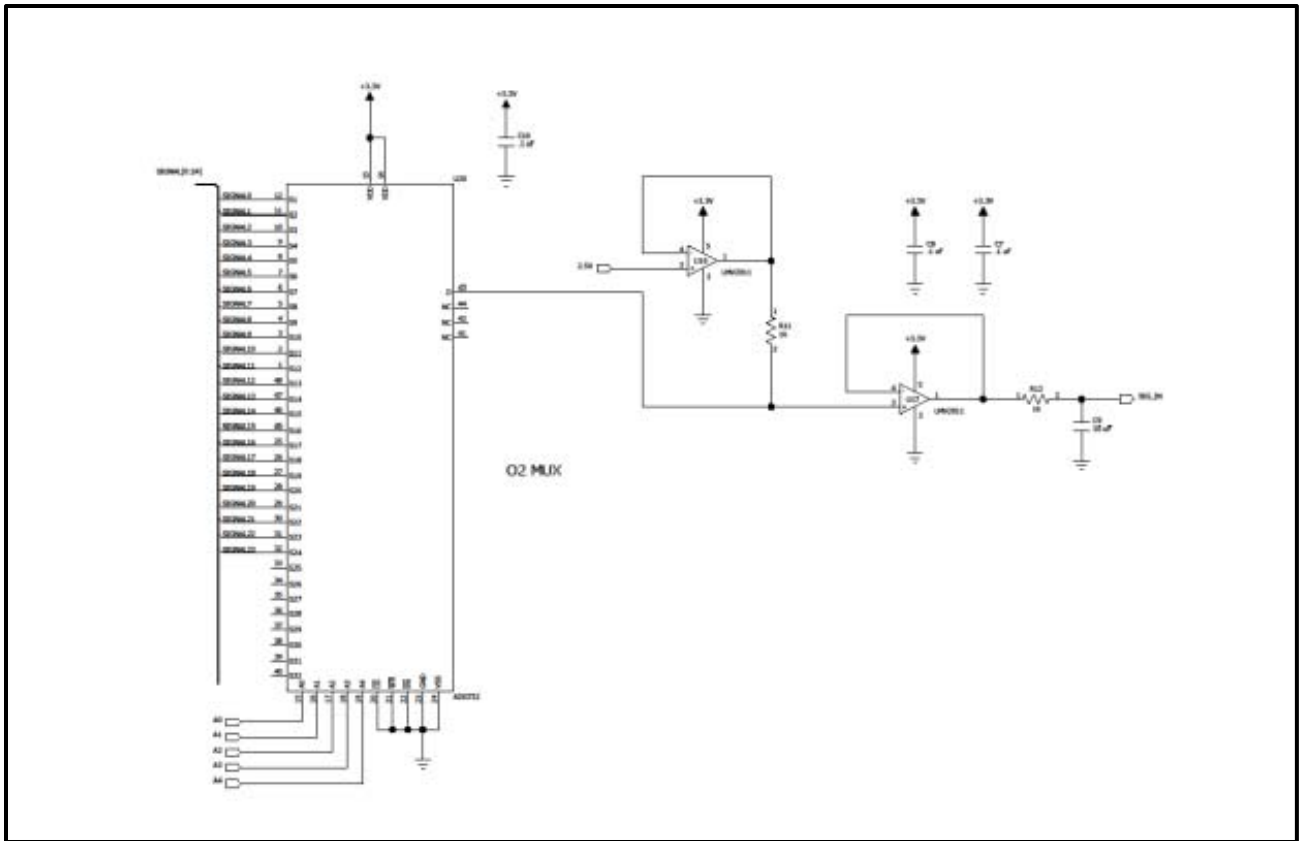


Fig. 10 (d) Multiplexer circuit

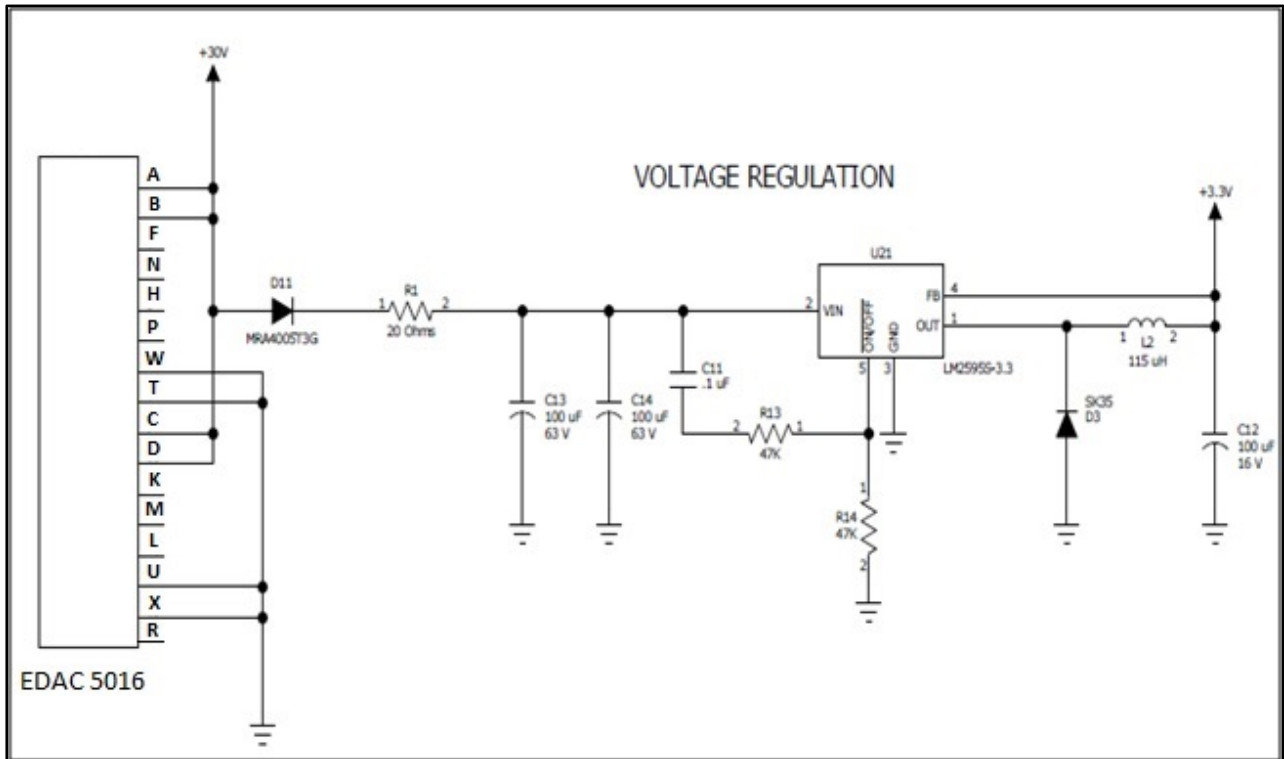


Fig. 10 (e) Voltage regulation circuit

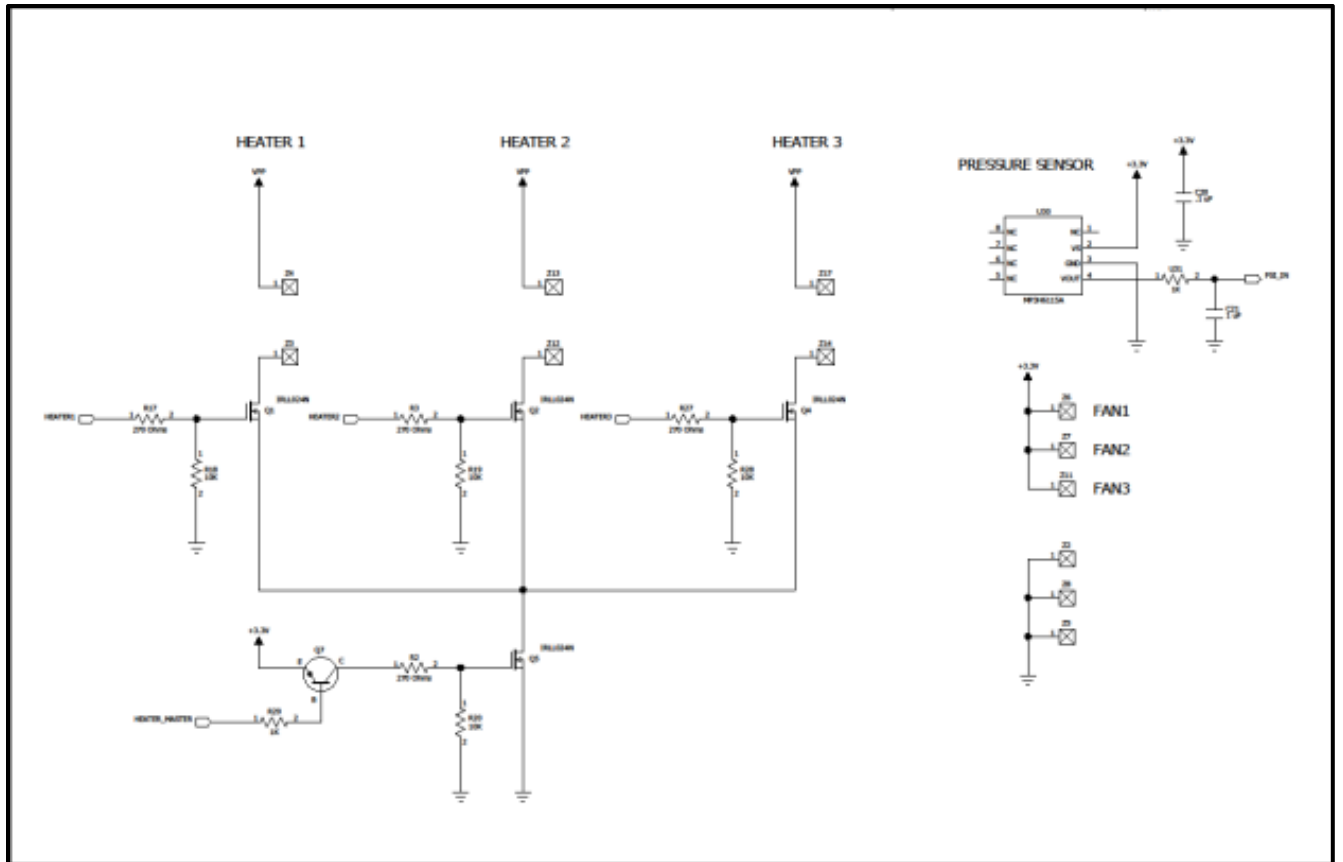


Fig. 10 (f) Circuit for three heaters, three fans and pressure sensor

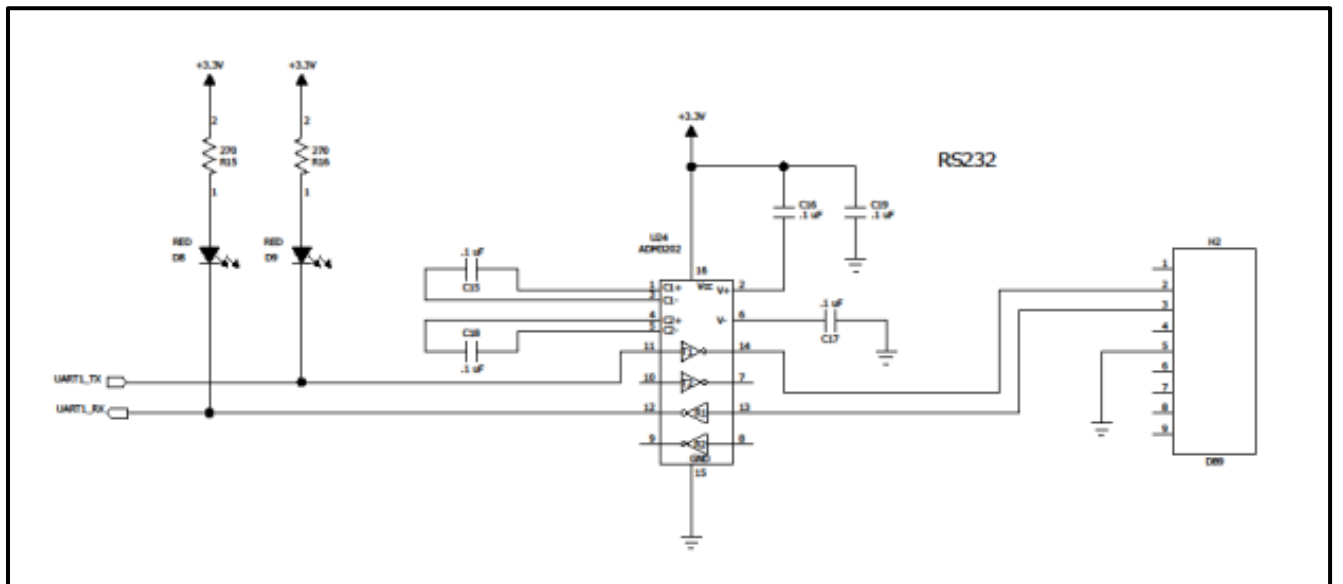


Fig.10 (g) Circuit for RS232

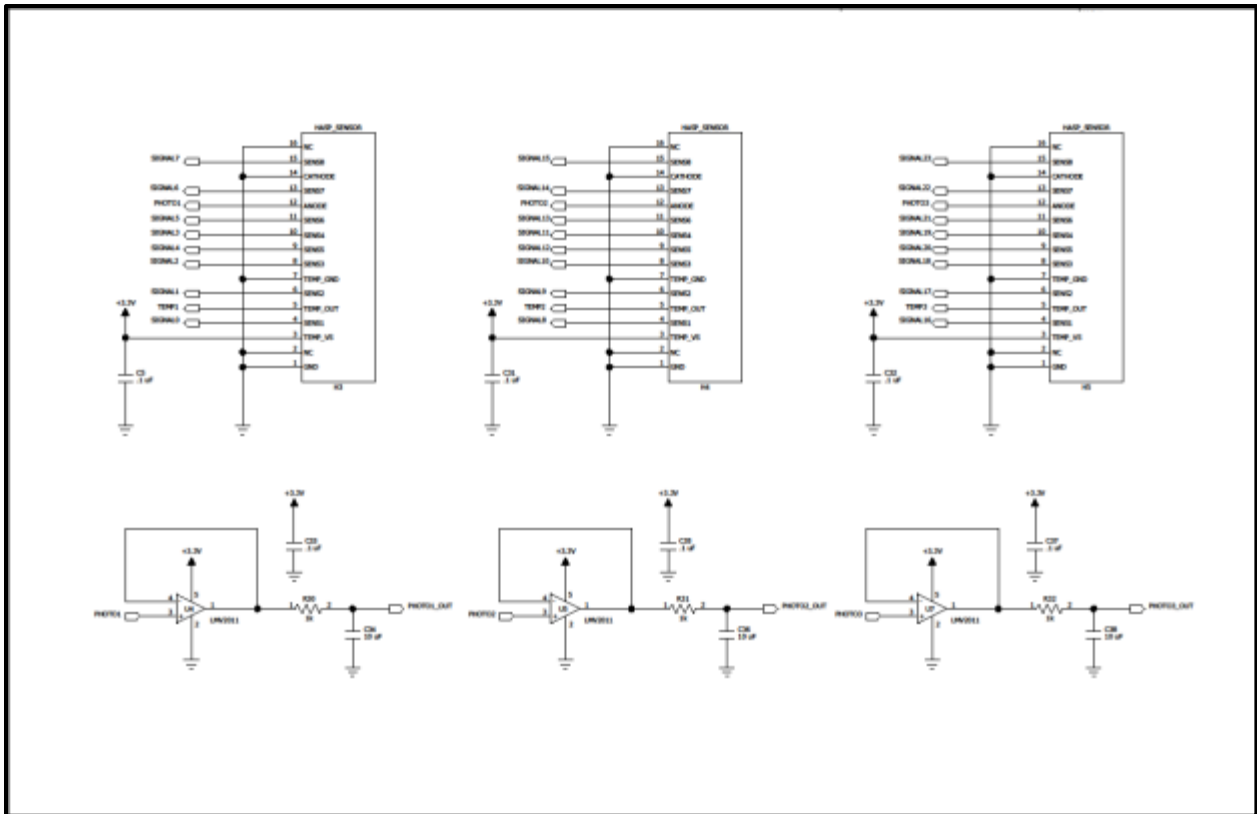


Fig.10 (h) Circuit for three ozone sensors boxes and three photo (light) sensors

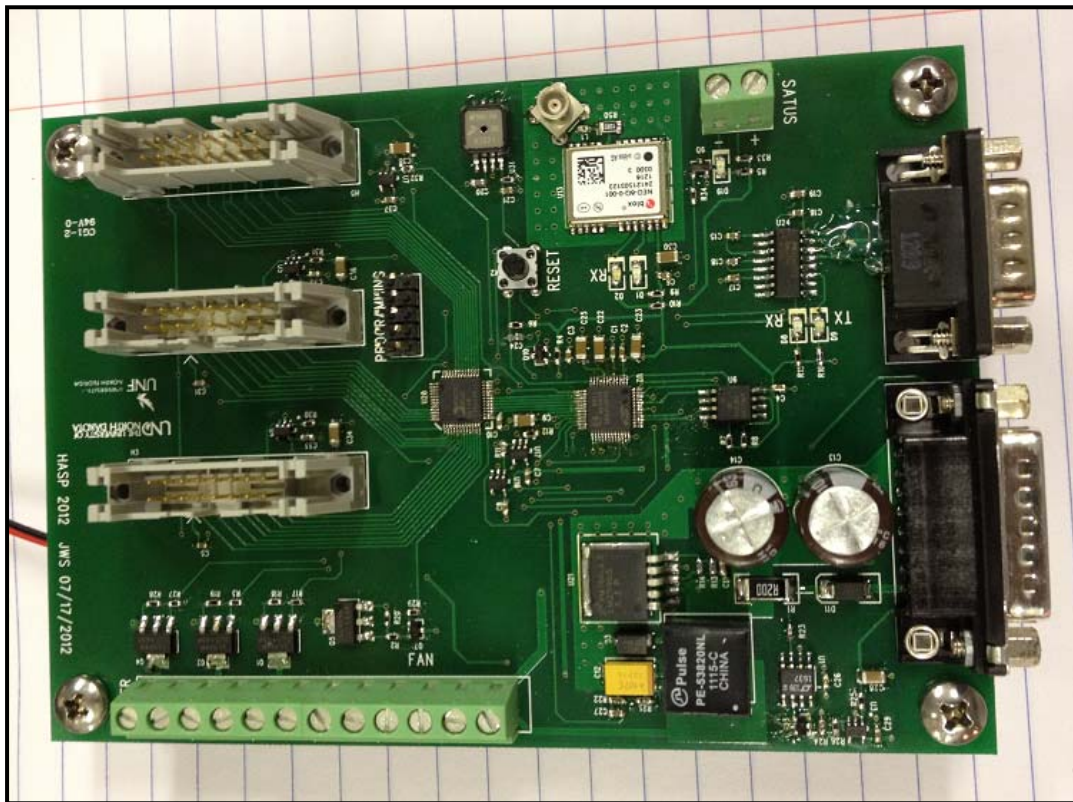


Fig. 10 (i) Picture of microcontroller PCBs

## 7. Integration of Payload and Thermal Vacuum Test

The payload body, sensors boxes and circuit board were interegrated at the the CSBF, Palestine during July 27 to August 1, 2013. Fig 11(a) to (g) shows pictures of various activites such as integration and testing of payload at CSBF, Palestine, TX.

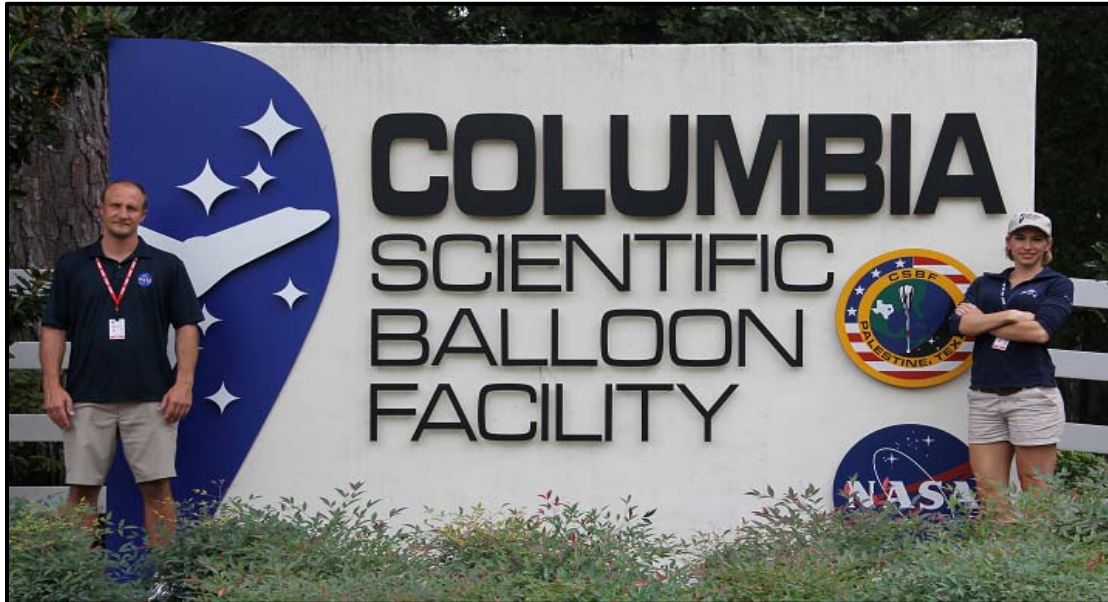


Fig. 11 (a) Ken and Brittany at CSBF, Palestine, TX

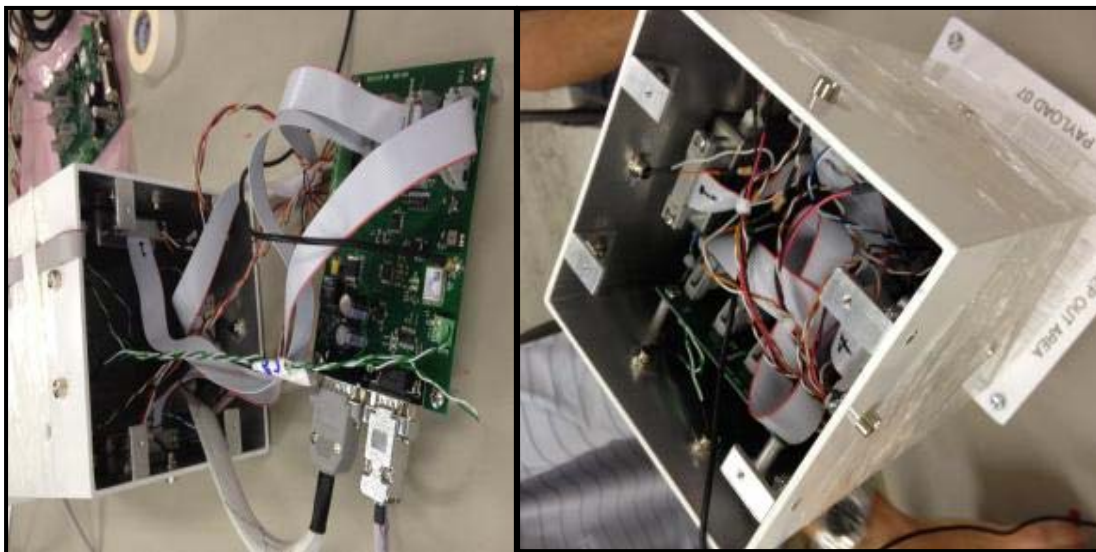


Fig. 11 (b) Inregration of sensors boxes, payload and PCB and Top view of payload



Fig. 11 (c) Dough Grainger (HASP), Ken and Brittany at the time of testing of the payload



Fig.11 (d) UNF team in front of the BEMCO thermal vacuum chamber

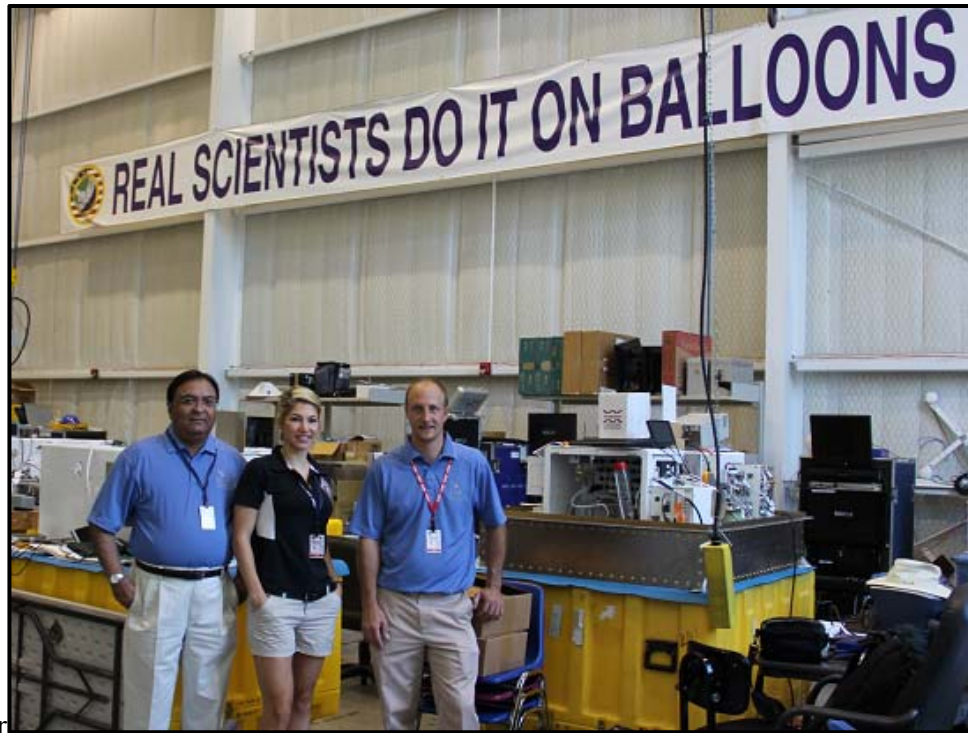


Fig.11 (e) Real scientists working at the NASA-CSBF balloon facility



Fig. 11 (f) Ken with Michael Stewart (HASP), Jill (CSBF) and Dr. Greg Guzik (Director, HASP) testing the uplink commands of payload during the thermal vacuum test.

Command	Hex Code	Description	Importance
RESET	7131	Reset System	Critical
HEAT_ON	7535	Turn Master Heater Switch Off	Critical
HEAT_OFF	7636	Turn Master Heater Switch On (default)	Critical
UBLOX_STREAM	7939	Stream GPS via Embedded GPS (default)	Critical
HASP_STREAM	7A3A	Stream GPS via HASP GPS	Critical

Fig. 11 (g) Uplink commands

The payload was tested in the BEMCO chamber, which is shown in Fig. 11(d) for high temperature (+40°C), low temperature (-40 °C), high pressure (1040 mbar), and low pressure (3 mbar). The measured current draw at 30 VDC is about 40 mA minimum, 425 mA maximum and 150 mA nominal. The payload successfully cleared the thermal vacuum test at the CSBF, Palestine, TX on Wednesday, July 30, 2014.

## 8. Launching of Payload

HASP2014 flight was successfully launched from CSBF, Fort Sumner, NM on Saturday, August 9, 2014 morning. Fig. 12 (a) shows the HASP 2014 balloon flight information, while fig. 12 (b) shows preparation of launch at the CSBF, Fort Sumner, NM.

<b>Balloon Flight Information</b>
▪ <b>Balloon Manufacturer: Winzen</b>
▪ <b>Balloon Type: Zero pressure</b>
▪ <b>Balloon Size: About 12 million cubic feet</b>
▪ <b>Parachute Diameter: 79 feet</b>
▪ <b>Flight Number: 649N</b>
▪ <b>Launch time :08/09/2014 13:25:13 UTC</b>
▪ <b>Launch location: NASA-CSBF, Ft Sumner, NM</b>
▪ <b>Float start :08/09/2014 15:39:00 UTC</b>
▪ <b>Termination :08/09/2014 21:17:00 UTC</b>
▪ <b>Float time :5:38</b>
▪ <b>Impact :08/09/2014 22:03 UTC</b>
▪ <b>Impact location :35° 31.20' N 111° 02.4"W</b>

Fig. 12 (a) HASP 2014 balloon flight information,



Fig. 12 (b) Preparation of launch at the CSBF, Fort Sumner, NM.

Fig. 12 (c) shows the launching of the balloon flight, while the picture of UND-UNF payload during flight in the stratosphere is shown in fig. 12(d) and fig. 12 (e).



Fig. 12 (c) Launching HASP2014 balloon flight at the CSBF, Fort Sumner, NM.

(Courtesy: Mr. Daniel Bowman, UNC, Chapel Hill)



Fig.12 (d) UND-UNF sensors payload in the starosphere

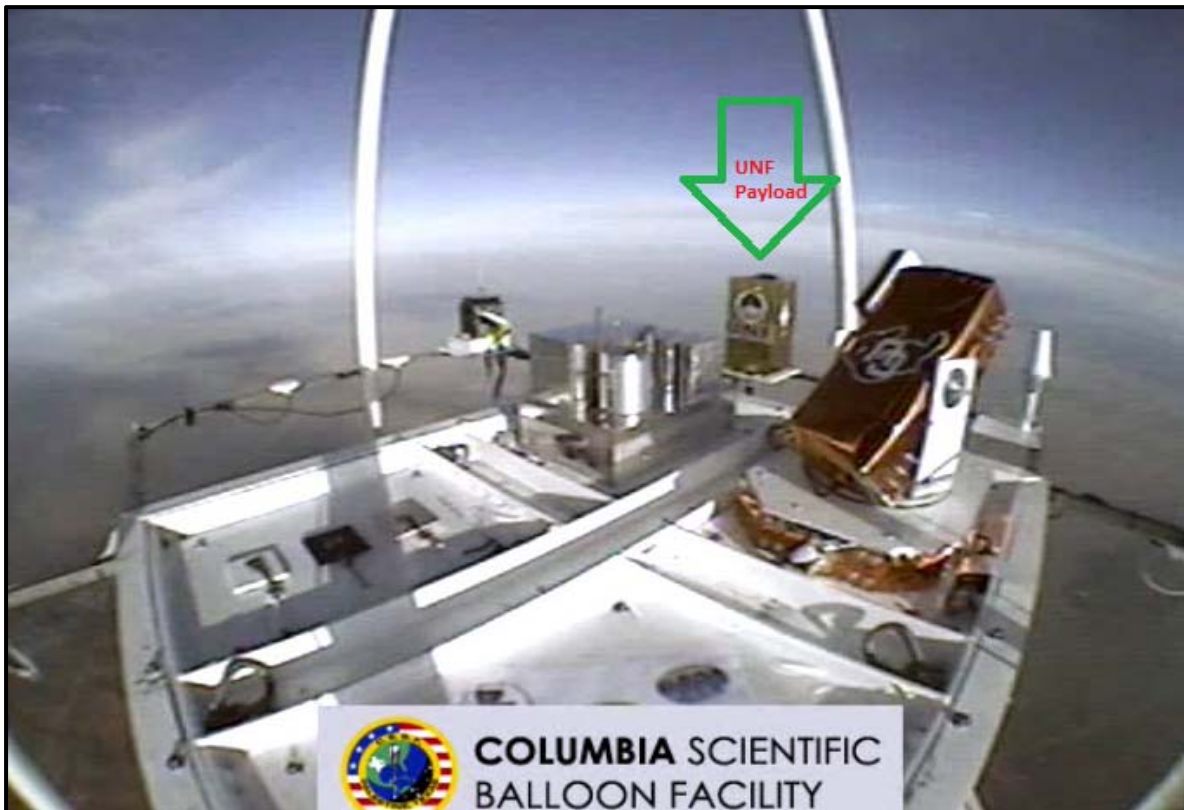


Fig.12 (e) UND-UNF sensors payload in the starosphere

The HASP 2014 flight was terminated on August 9, 2014. Fig. 13 (a) shows the flight path of the balloon on the Google map.

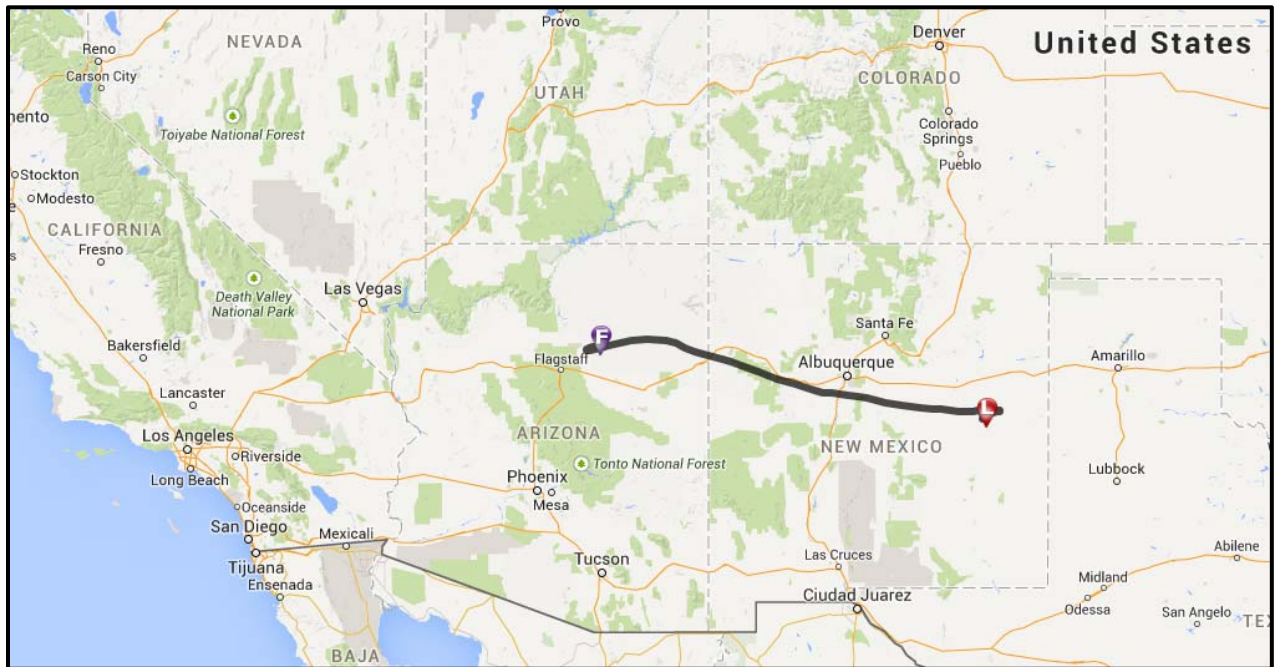


Fig.13 (a) Flight path of the balloon flight on the Google map

The HASP balloon flight was terminated and then impacted near Flagstaff, Arizona. The distance between Fort Sumner, NM and Flagstaff, AZ by the Route I-40 W is about 481 miles. Fig. 13 (b) shows the impact of HASP on the ground after termination, while fig. 13 (c) shows the recovery team member with HASP. The UND-UNF payload was narrowly escaped from the direct hit on the ground.



Fig. 13 (b) Impact of HASP on the ground and (c) the recovery team member with HASP.

(Courtesy: HASP)

## 9. Results and Discussions:

### 9.1 How ozone profile measured in the Starosphere?

Fig. 14 shows various steps for the detection of ozone by the sensors payload during the flight.

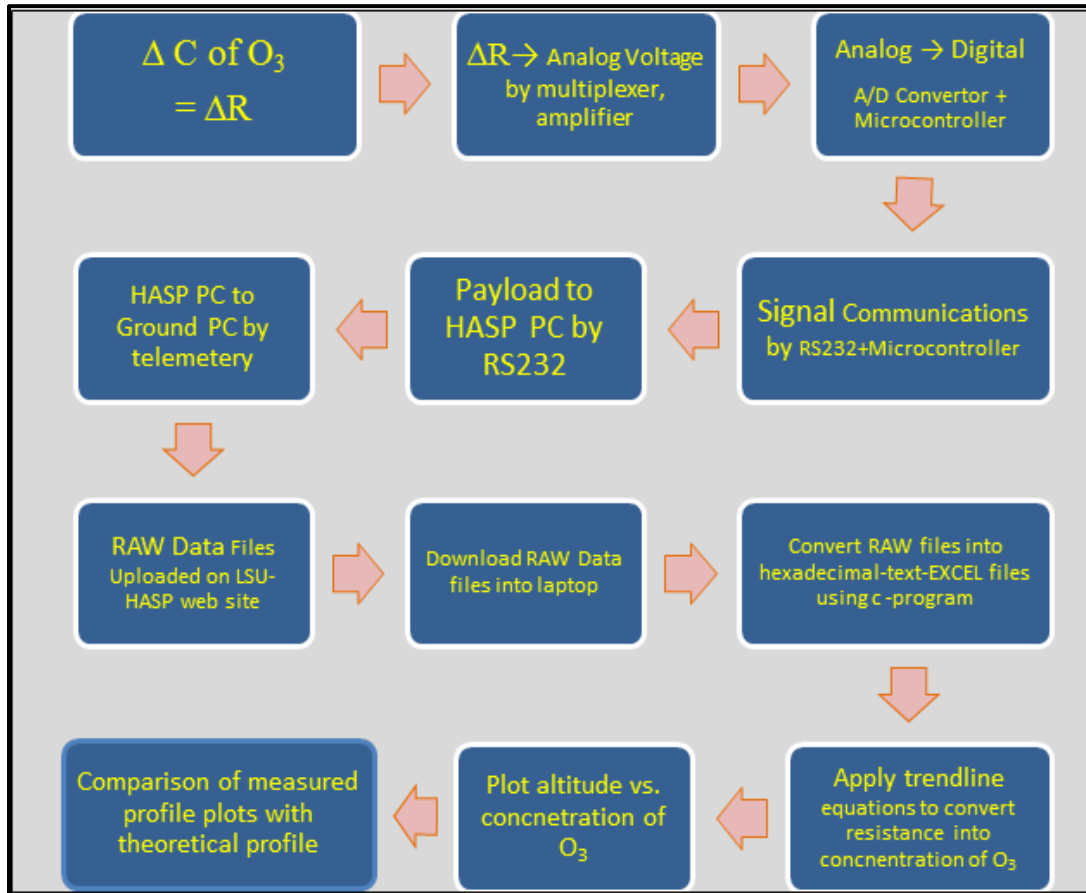


Fig.14 Steps for the detection of ozone by the payload

During the flight, UND-UNF sensors payload measured the ozone profile. The payload sent data files of 25 KB every 18 minutes during the flight time through the NASA-HASP computer and was uploaded on the HASP website. We downloaded all the RAW data files, and converted RAW files into one EXCEL file using the software program. It was found that the sensors, hardware and software worked very smoothly. There was no need to upload the special commands to reboot the payload system during the flight.

### 9.2 Balloon Flight Profile and Response of Pressure Sensor

Fig. 15 (a) shows the HASP 2014 balloon flight profile. The altitude profile was measured by the initially by HASP GPS during ascend and float and then by UND-UNF GPS during descend. This flight profile has few times missing data due to switch over of our GPS to HASP GPS during ascending as well as no power and / or communication after termination and impact. We are thankful to Mr. Doug Granger (LSU-HASP) for sharing altitude data.

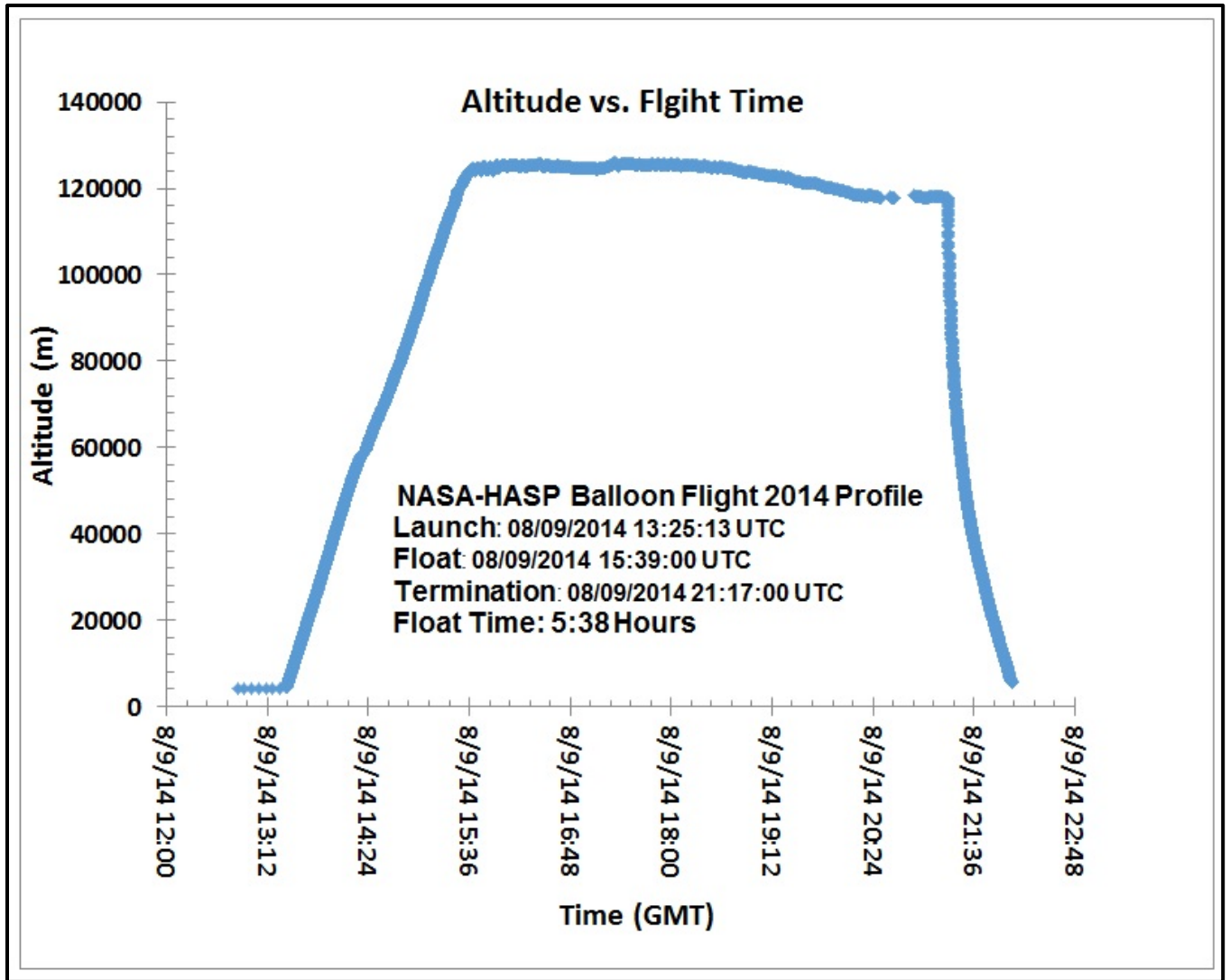


Fig.15 (a) HASP2014 flight profile

Fig.15 (b) shows the variation of pressure with the altitude during the flight. Pressure was measured by a pressure sensor mounted on the PCB of the payload. The red color arrow shows data generated during ascending of the balloon, while green arrow shows the data generated during descending of the HASP after termination of balloon.

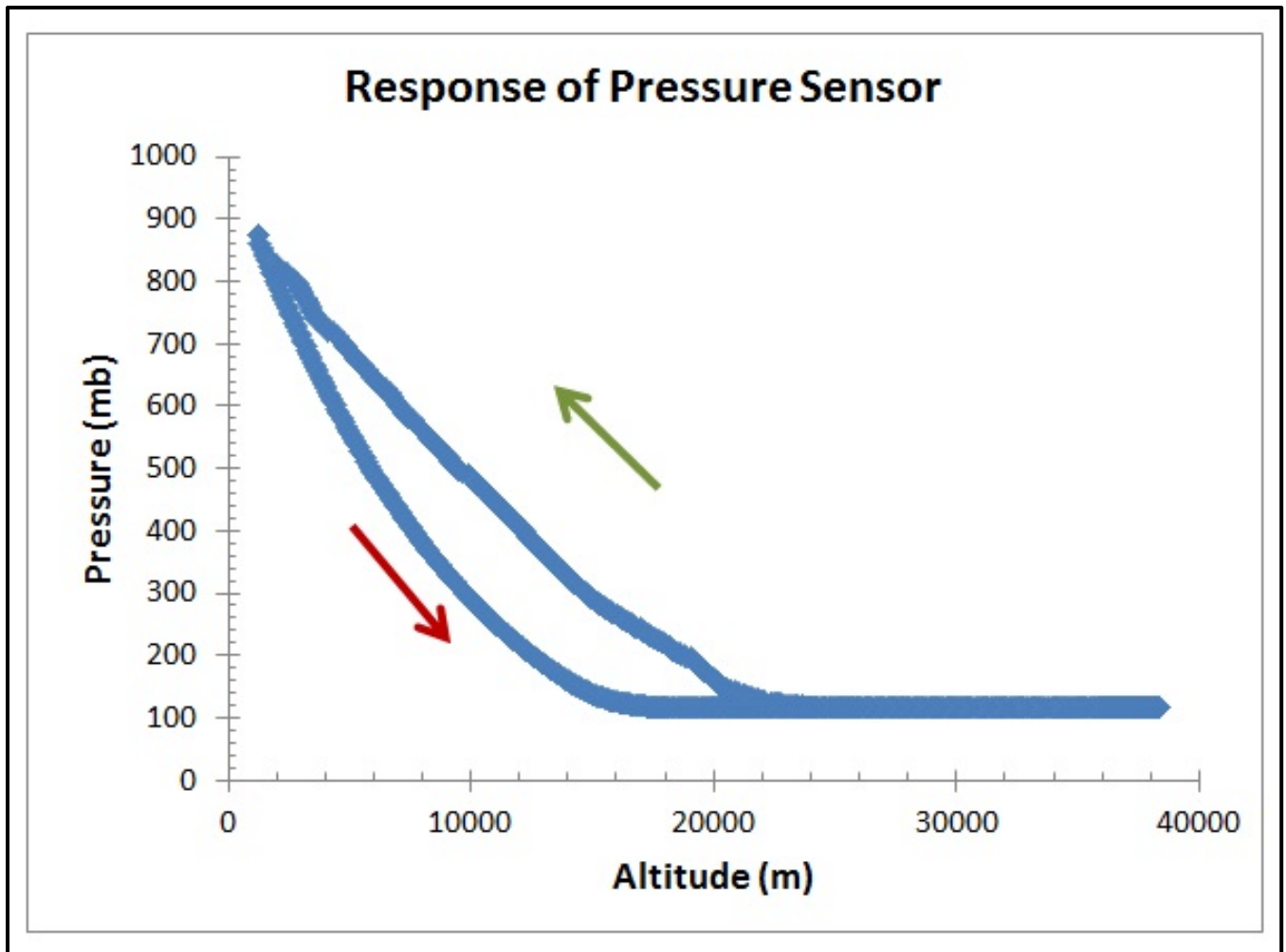


Fig.15 (b) Variation of pressure with altitude

It was found that the pressure was decreased with increase of the altitude up about 15 km and then nearly saturate with increase of altitude up to the float. The saturation of pressure around 100 mbar was due to the technical limitation of our pressure sensor. We will replace this pressure sensor with one having lower mbar range in the next balloon flight. .

### 9.3 Power budget during the flight

Fig. 16(a) shows the voltage applied to the payload during the flight. It was found that applied voltage remain nearly constant about 3300mV. The current drawn by the payload during the flight is shown in fig. 16(b). Payload draw minimum 30 to 40 mA when all three heaters were off, while maximum about 380 mA when all three heaters were on. The power budget was maintained under the upper limit of HASP requirement during the flight.

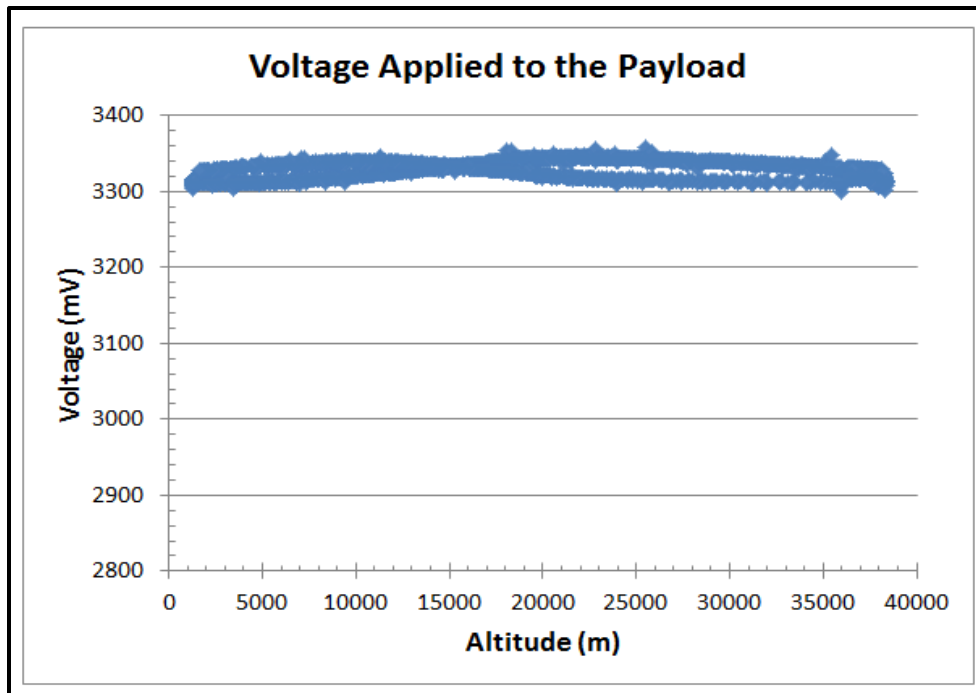


Fig.16 (a) Voltage applied to the payload during the flight.

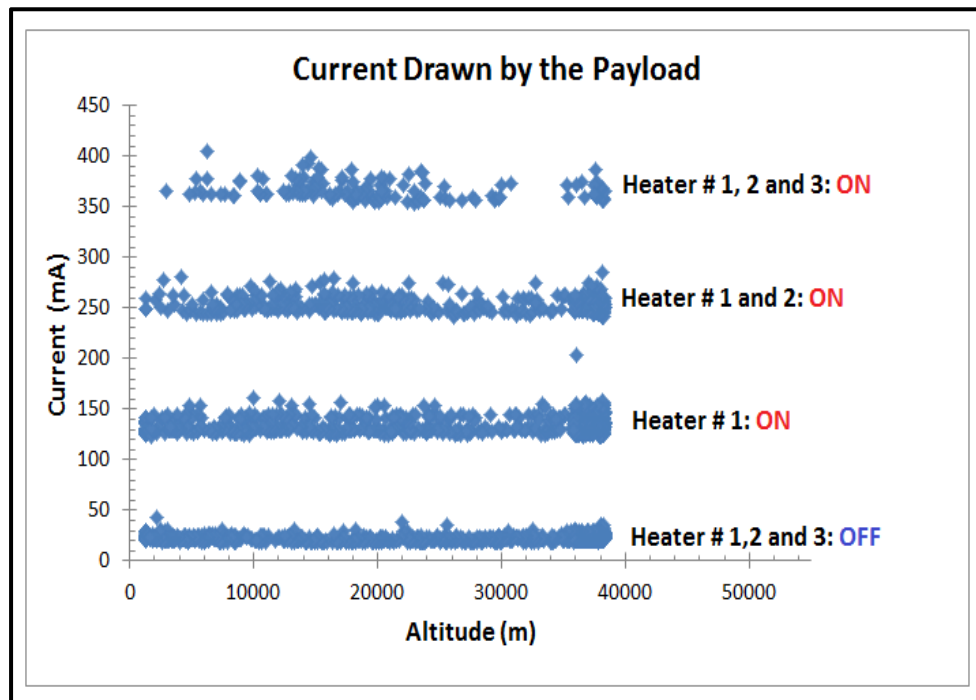


Fig.16 (b) Current drawn by the payload during the flight

### 9.4 Thermal stability of the payload

The variation of temperature of ozone sensors box #1, 3 and 4 with altitude during the flight is shown in fig.17 (a), (b) and (c), respectively. The temperature of sensors was controlled in the range of  $302 \pm 5.7$  K using an On-Off controller, a polyimide flexible heater (MINCO make) and

a temperature sensor TMP 36). Temperature of sensors was well controlled during the most of time of the flight. Some of data were missing due to the issue of mixing data. Table-1 shows the measured average temperature, standard deviation and one sigma standard error of temperature of sensor box#1, box#3 and box#4.

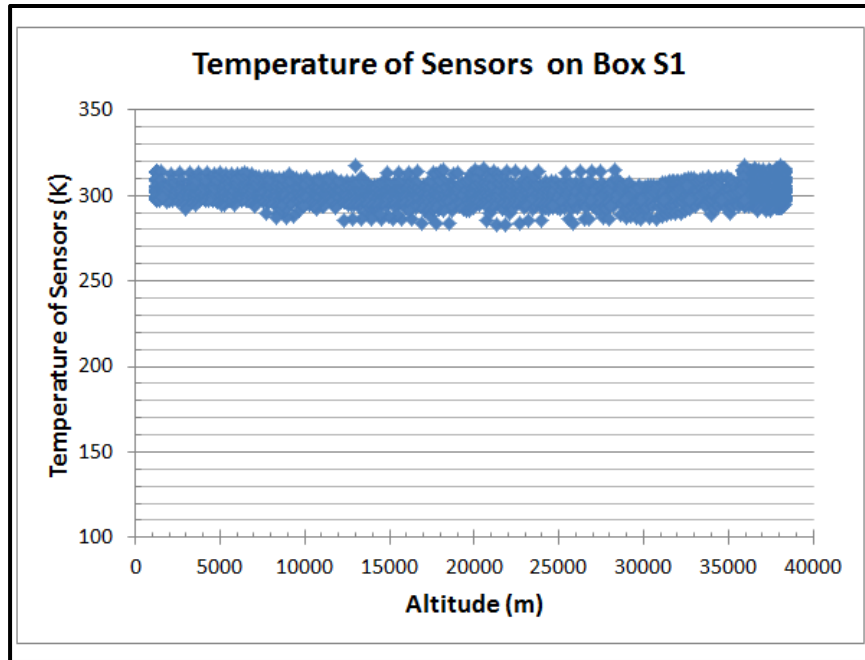


Fig.17 (a) Temperature of ozone sensors box#1

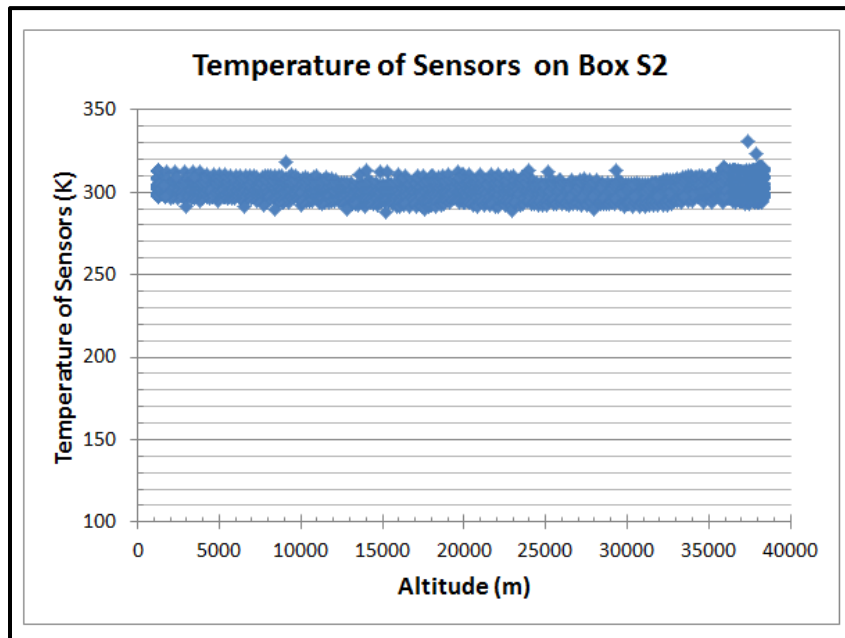


Fig.17 (b) Temperature of ozone sensors box#3

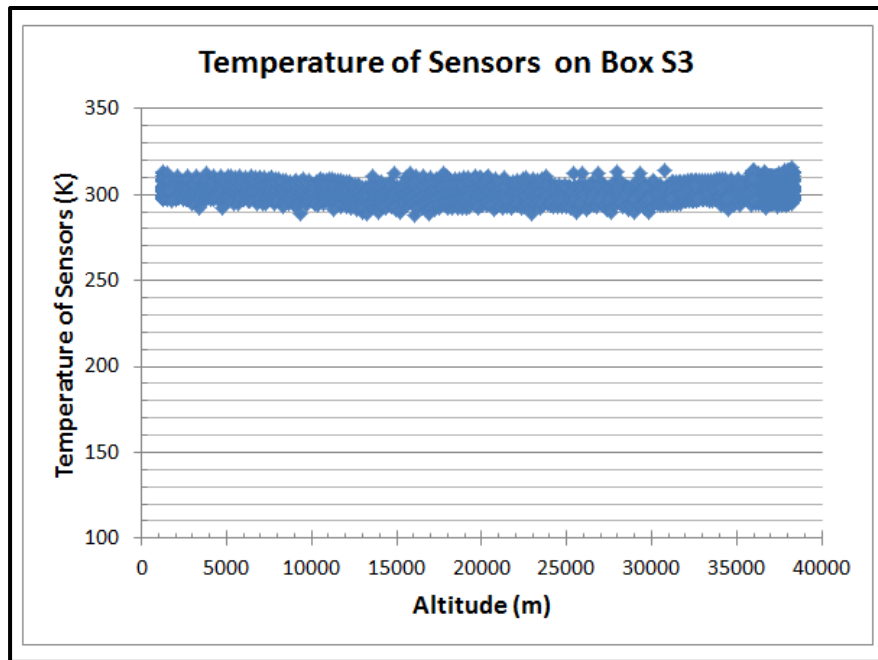


Fig.17 (c) Temperature of ozone sensors box#4

Sensors Box #	1	3	4
Average Temperature (K)	302.1	302.0	301.8
Standard Deviation (K)	5.7	5.7	5.3
Standard Error (K)	0.1	0.1	0.1

Table1. Average temperature and standard deviation of temperature of sensors array 1, 3 and 4 during the flight.

### 9.5 Measurements of photovoltage profile during the flight

The variation of photovoltage generated by the photo diodes mounted on sensor box #1, 3 and 4 during the flight is shown in fig 18 (a), (b) and (c), respectively. It was observed that measured photovoltage was larger in the altitude range about 12000 to 30000 m. The larger photovoltage confirmed the presence of ultra violet Sun light. In the presence of that UV light oxygen converted into ozone gas.

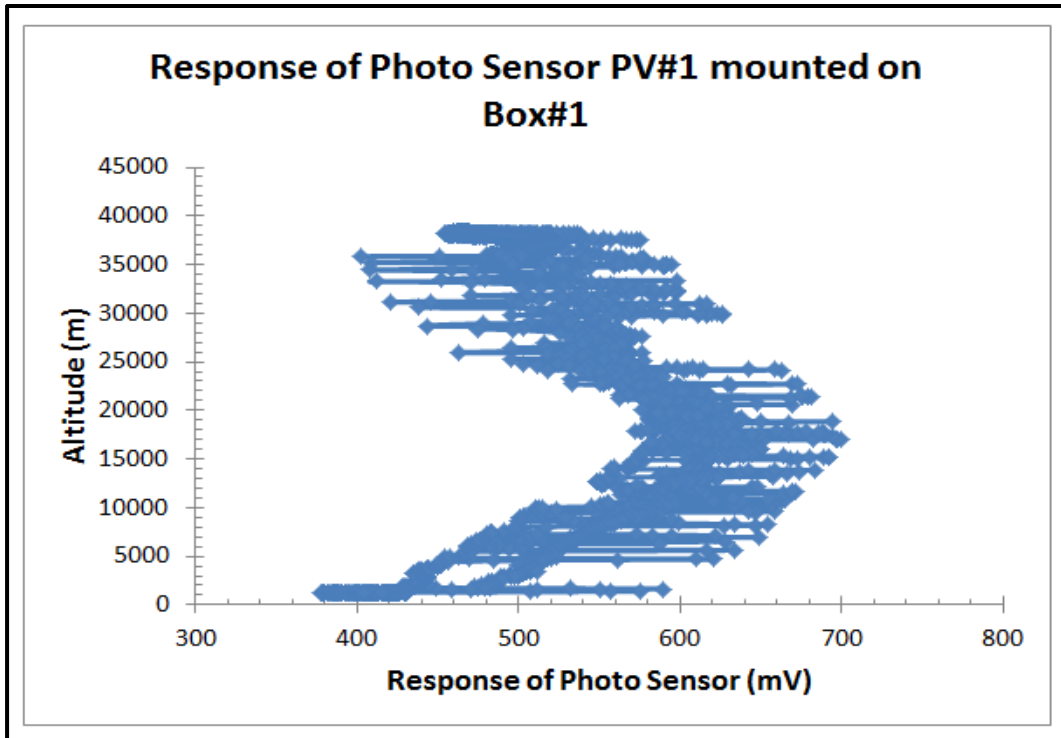


Fig.18 (a) Variation of photovoltage on sensor box#1

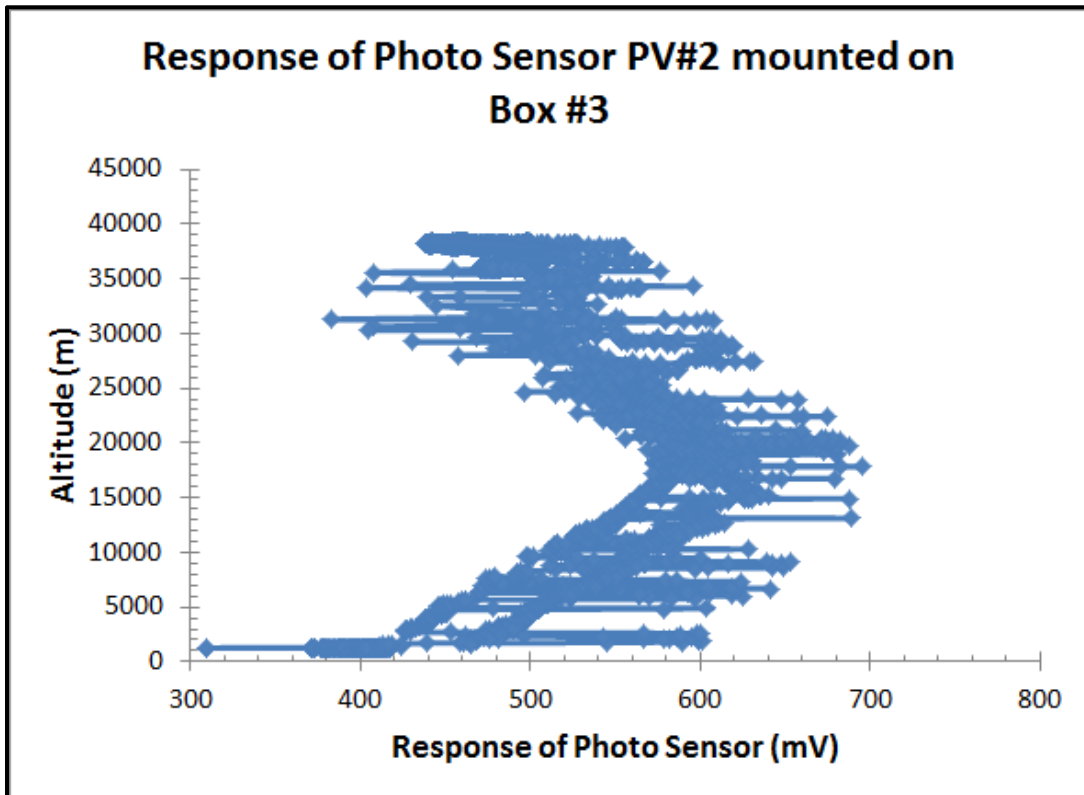


Fig.18 (b) Variation of photovoltage on sensor box#3

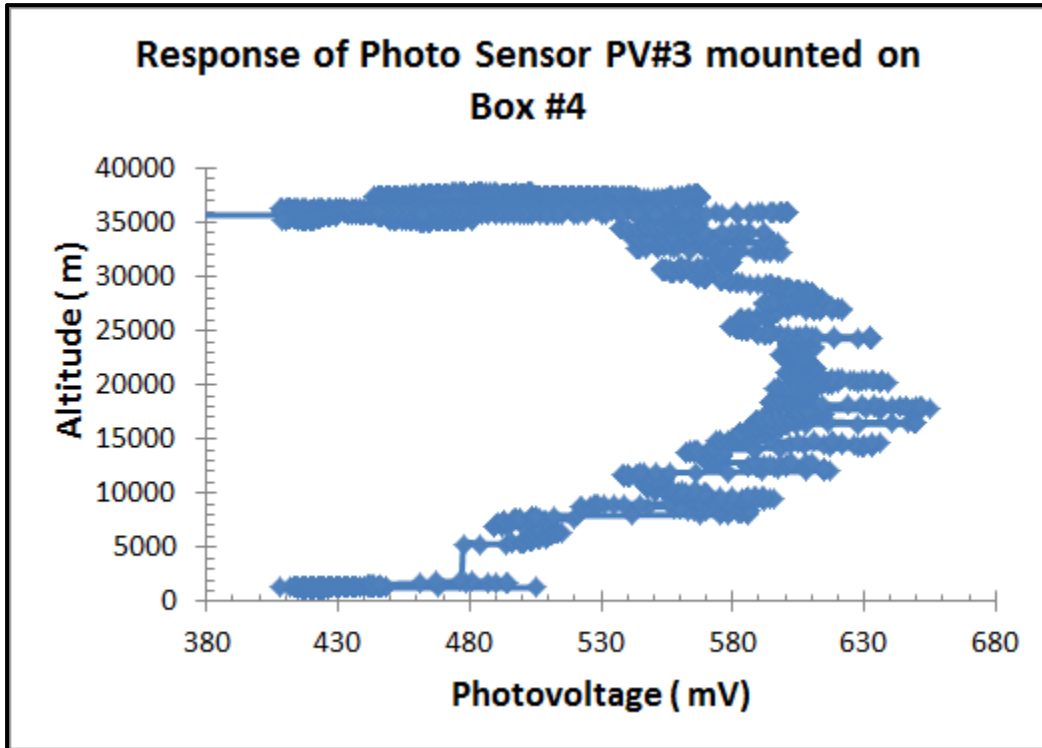


Fig.18 (c) Variation of photovoltage on sensor box#4

## 9.6 Discussion of Response of Gas Sensors Profiles

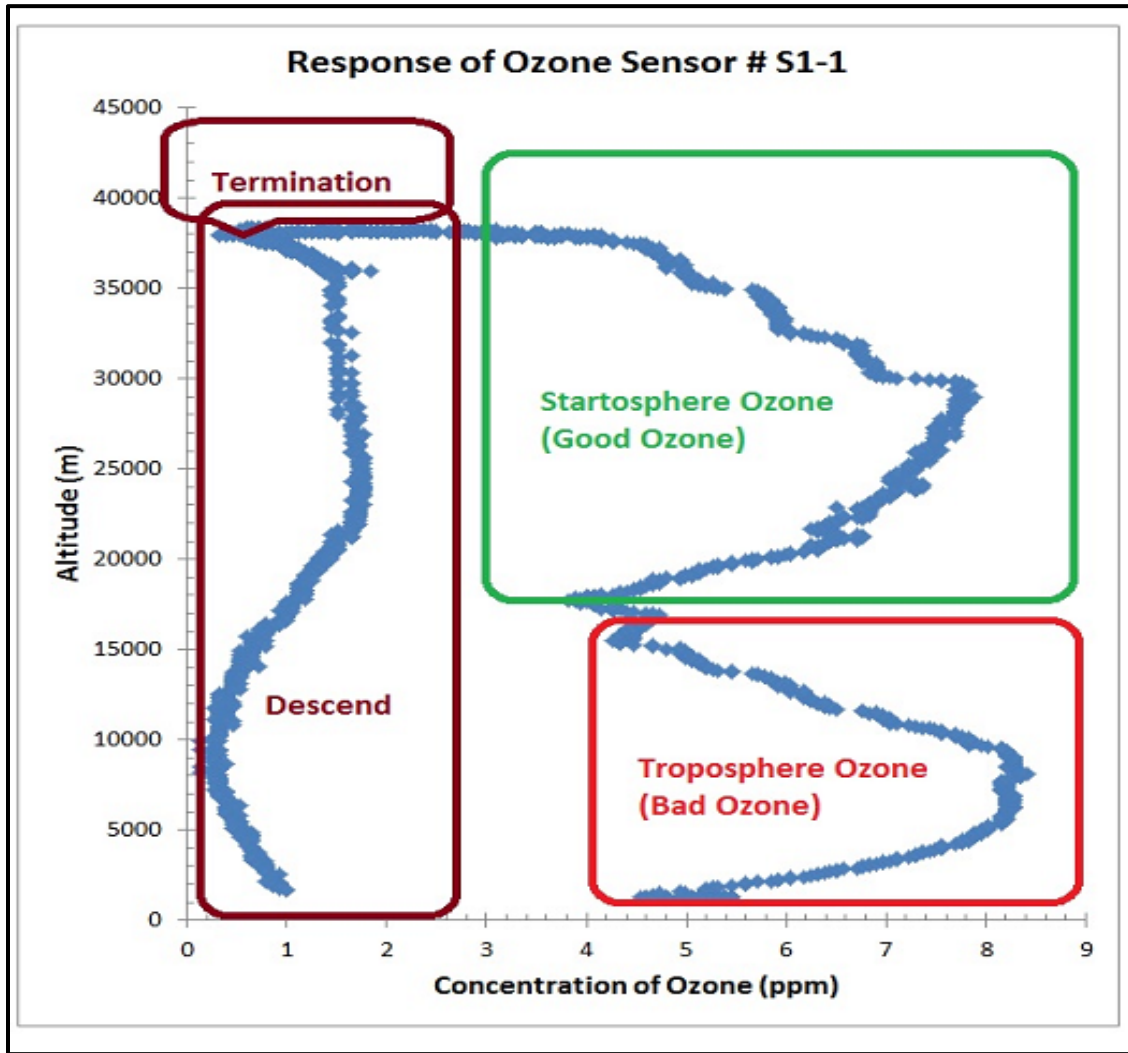


Fig.19 (a) Response of ozone sensor of **Box#1** (S1#1) with complete range of altitude

Sensor # S1-1 was randomly picked for the discussion of response of sensor with the entire range of altitude of balloon. Sensors of Box-1 were made of improved version of nanocrystalline ITO thin films compare to our previous balloon flights. These sensors have better selectivity and sensitivity with ozone gas.

Small peak of ozone was observed during ascending of balloon flight at the altitude below 15000 m. This range of altitude is in the troposphere. This small ozone peak is known as the bad ozone, which is mainly due to the generation of smog in the early morning due to pollution by the automobile vehicles and industries. The bigger peak of ozone is observed at altitude above 15000 m and up. This is due to the ozone in the stratosphere. This ozone is known as good ozone. In the presence of ultra violet light from Sun, oxygen converted into ozone gas. The concentration of ozone is higher in the middle of stratosphere in the presence of ultra violet light. Ozone is oxidizing gas and its concentration depends on amount of available Sun light. Upon adsorption of charge accepting molecules at the vacancy sites from ozone oxidizing gas, the electrons are

effectively depleted from the conduction band of n-type Indium tin oxide (ITO) semiconductor sensor. Thus, this leads to an increase in the electrical resistance of n-type ITO gas sensor. At the maximum float of balloon, the concentration of ozone should be constant, but it may vary due to mixing ratio and availability of ultra violet rays from the sunlight. After termination of balloon, the payload again entered into the middle of stratosphere, the resistance of sensor should again increase and then decrease. The data on plot needs to zoom in to find this observation. That peak is not enough large to see in the fig.2 due to fact that the payload was dropping at the higher speed than that of the upward journey and none availability of ultra violet during night time. This region is labeled as “Descend” in the fig.2. Note that there was no effect of cold temperature on sensor because the temperature of gas sensors was controlled and maintained to about 293 to 308 K. The amount of anthropogenic ozone in this zone is very low compared to that of good ozone in the stratosphere. All eight sensors (S1#1 to S1#8) of box-1 have similar observation of ozone peak in the stratosphere.

Response of sensors of box-3 was also similar to box-1. Response of sensor #S3-4 of Box-3 is shown in Fig.19 (b). Sensors of Box-3 were made of nanocomposite of ZnO + ITO thin films. Both sensors boxes #1 and 3 have good selectivity of ozone gas in the stratosphere (part-II) compare to that other pollutant gases in the atmosphere and troposphere (part-I).

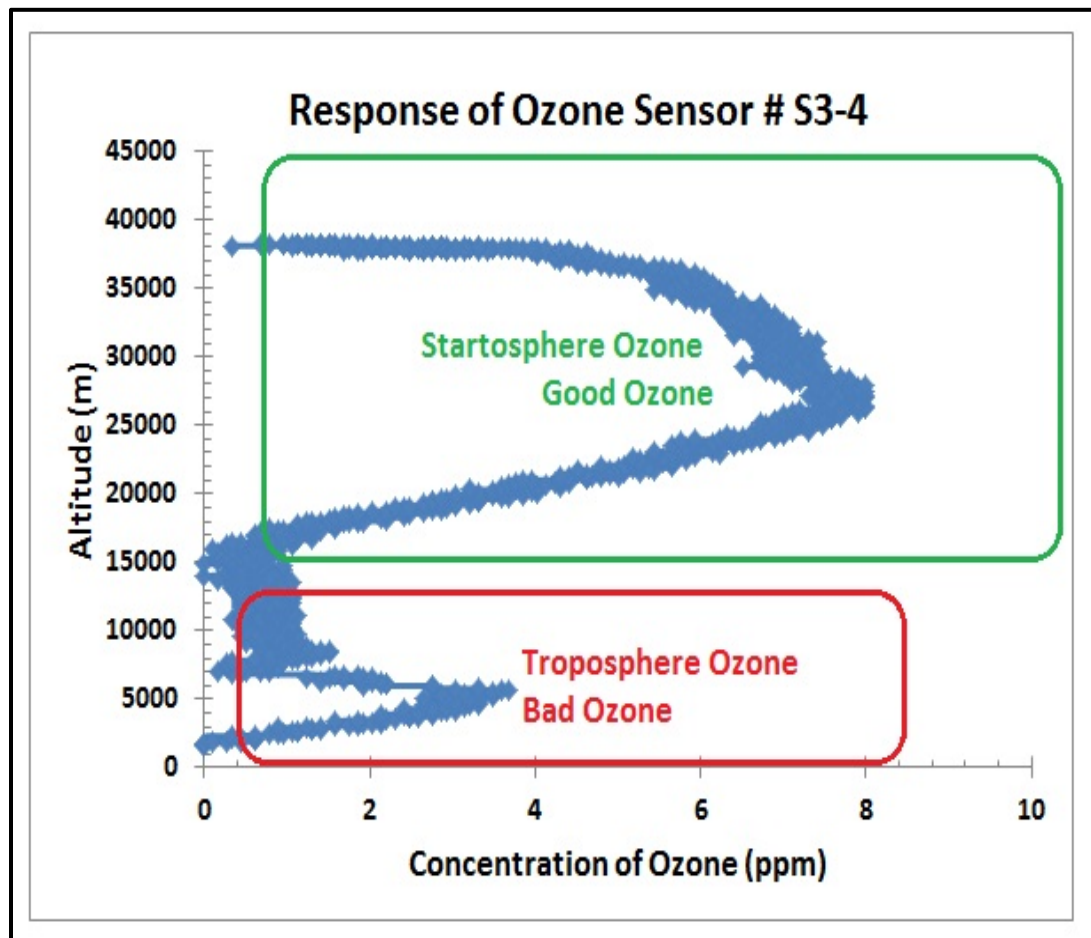


Fig.19 (b) Response of ozone sensor of **Box# 3** (sensor S3#1) with entire range of altitude

Based on this discussion and fact, we filtered out the data of troposphere and data generated after termination of flight or during descend and worked further over the data generated in the stratosphere only.

Fig.19 (c) shows the plots of response of reducing gases sensors # S4-1 to # S4-8. Sensor array was made of  $WO_3+ITO$  nanocrystalline thin film. These sensors are n-type semiconductor. In the presence of reducing gases, its resistance should be decreased. It was observed that resistance of sensor decreases as the altitude increases. There is no observation of peak of oxidizing ozone gas in the stratosphere range. Resistance of sensor shows very small variation during the float journey. This may be due to the presence of very low pressure at the higher altitude. The resistance of sensor was nearly same during descend. The response of reducing gases sensor was measured first time. All 8 sensors (S4-1 to S4-8) have shown the similar nature of response. Reducing gases consist of mixture of more than one or two gases. Calibration of each gas may not correctly apply to the measured data because of the continuous variation of mixing ratio and pressure and hence require further study. We therefore have not presented the calibration of plots of the box#4 in this report.

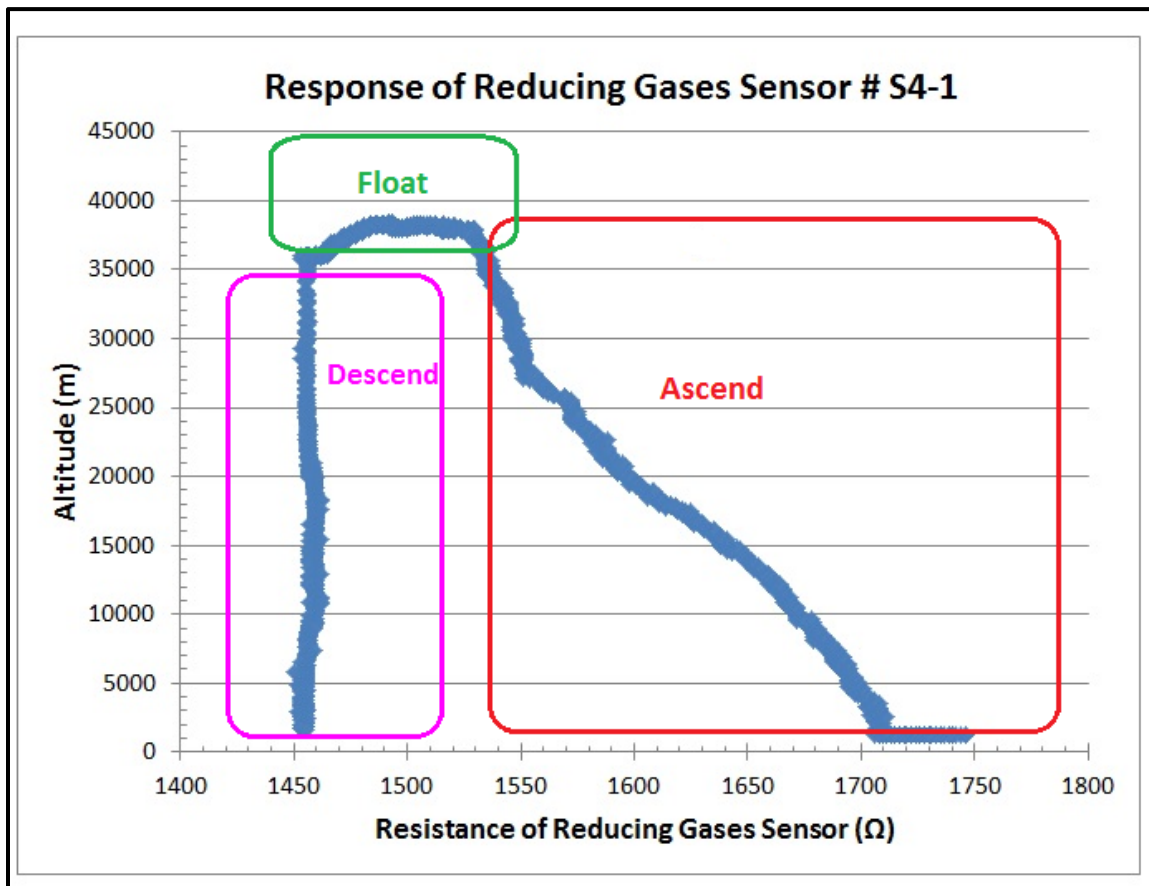


Fig.19 (c) Response of ozone sensor of **Box#4** (sensor S4#6) with complete range of altitude

## 9.7 Response of Ozone Sensors during the Flight

### (i) During ascending

Variation of ozone concentration with time during ascending of the balloon through the stratosphere is shown in fig.19 (e). The measured concentration of ozone by sensor was continuously increased towards the maximum concentration of ozone in the middle of stratosphere, which is shown in fig. 19 (e).

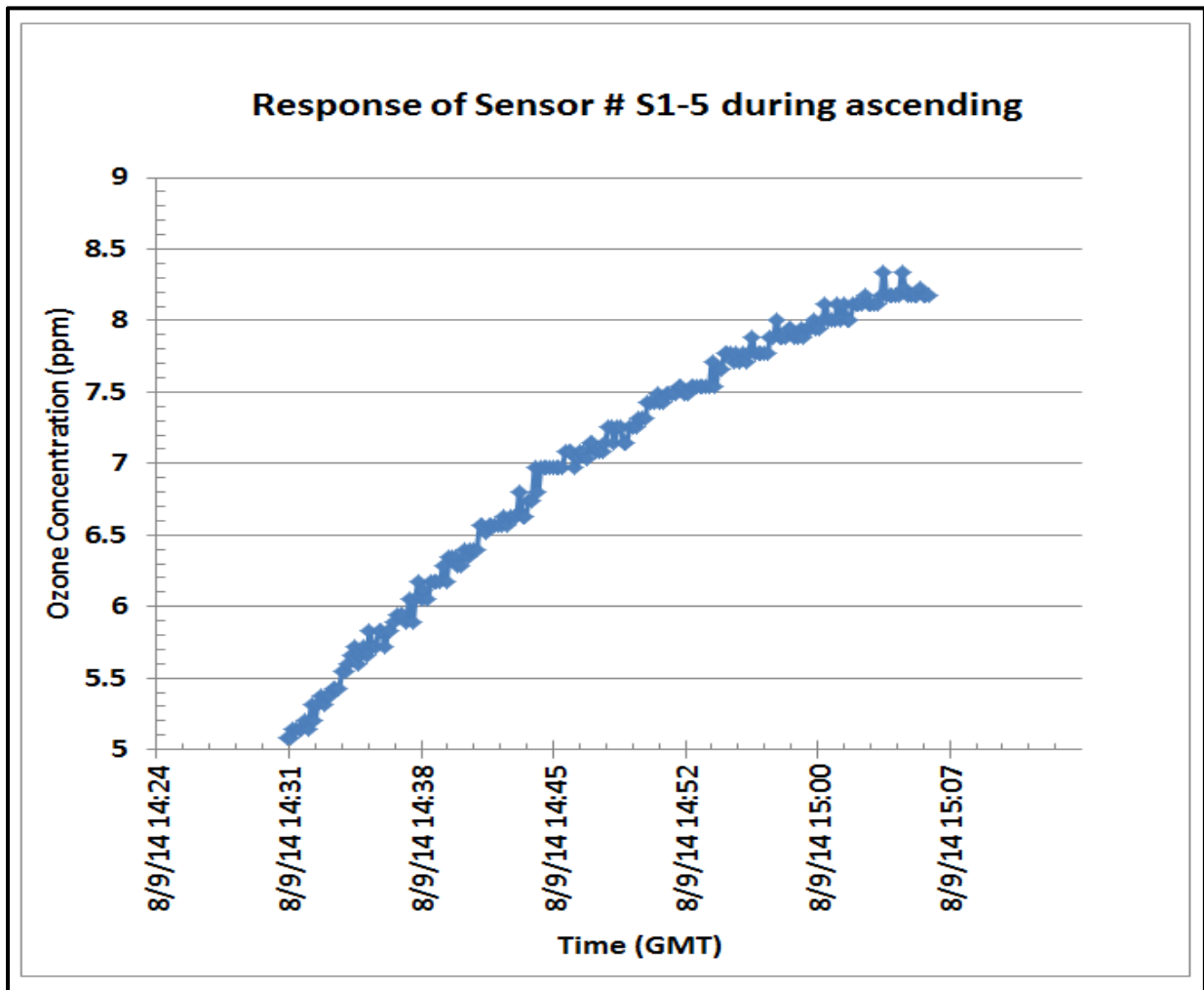


Fig.19 (e) Variation of concentration of ozone just before float with time

### (ii) During float

Variation of ozone concentration with time during float is shown in fig.19 (f). The measured concentration of ozone by sensor was slowly decreased with time during these time period, which is shown in fig. 19 (f). The slow decrease in ozone may be due to the fact that the decreasing of amount of UV light near sensor to convert oxygen into ozone and mixing ratio.

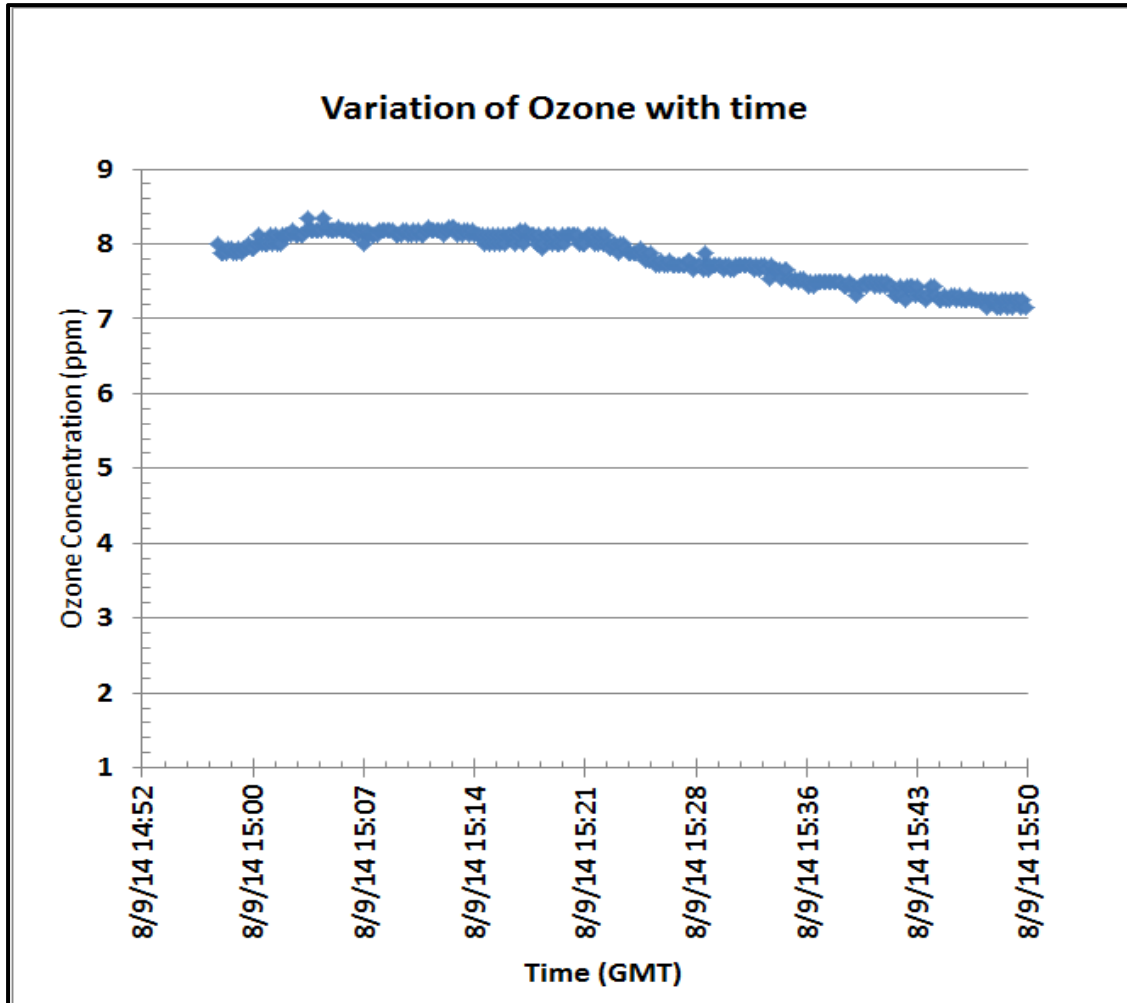


Fig.19 (f) Variation of altitude of balloon during float with time

**(iii) During descending**

Variation of ozone concentration with time during descend is shown in fig.19 (g). The measured concentration of ozone by sensor was decreased with time during these time period in stepwise, which is shown in fig. 19 (g). The decrease in ozone may be due to the fact that the decreasing of amount of UV light near sensor to convert oxygen into ozone and sudden increase of downward speed of payload on the parachute ride.

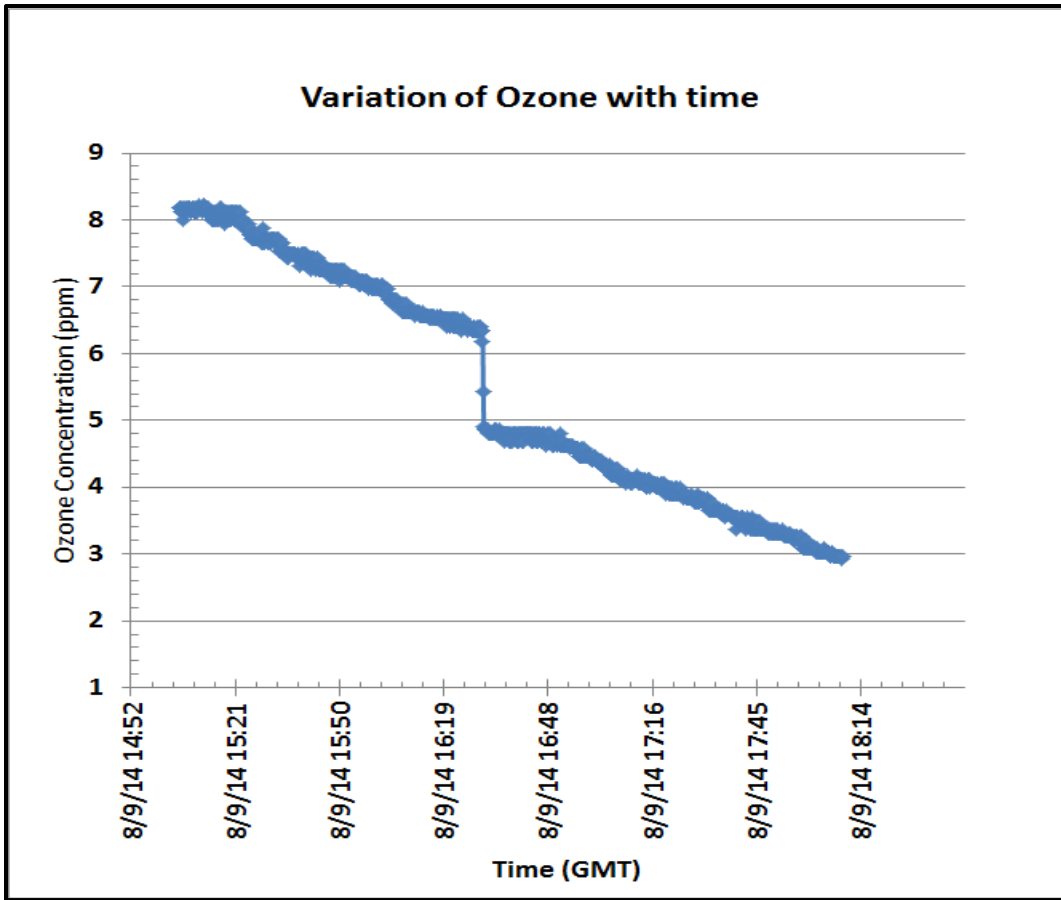


Fig.19 (g) Variation of concentration of ozone during descend with time

Response of sensors box #1 and 3 with the altitude is shown in fig.20 (a) and (b). We focused mainly the stratosphere range to measure the ozone profile.

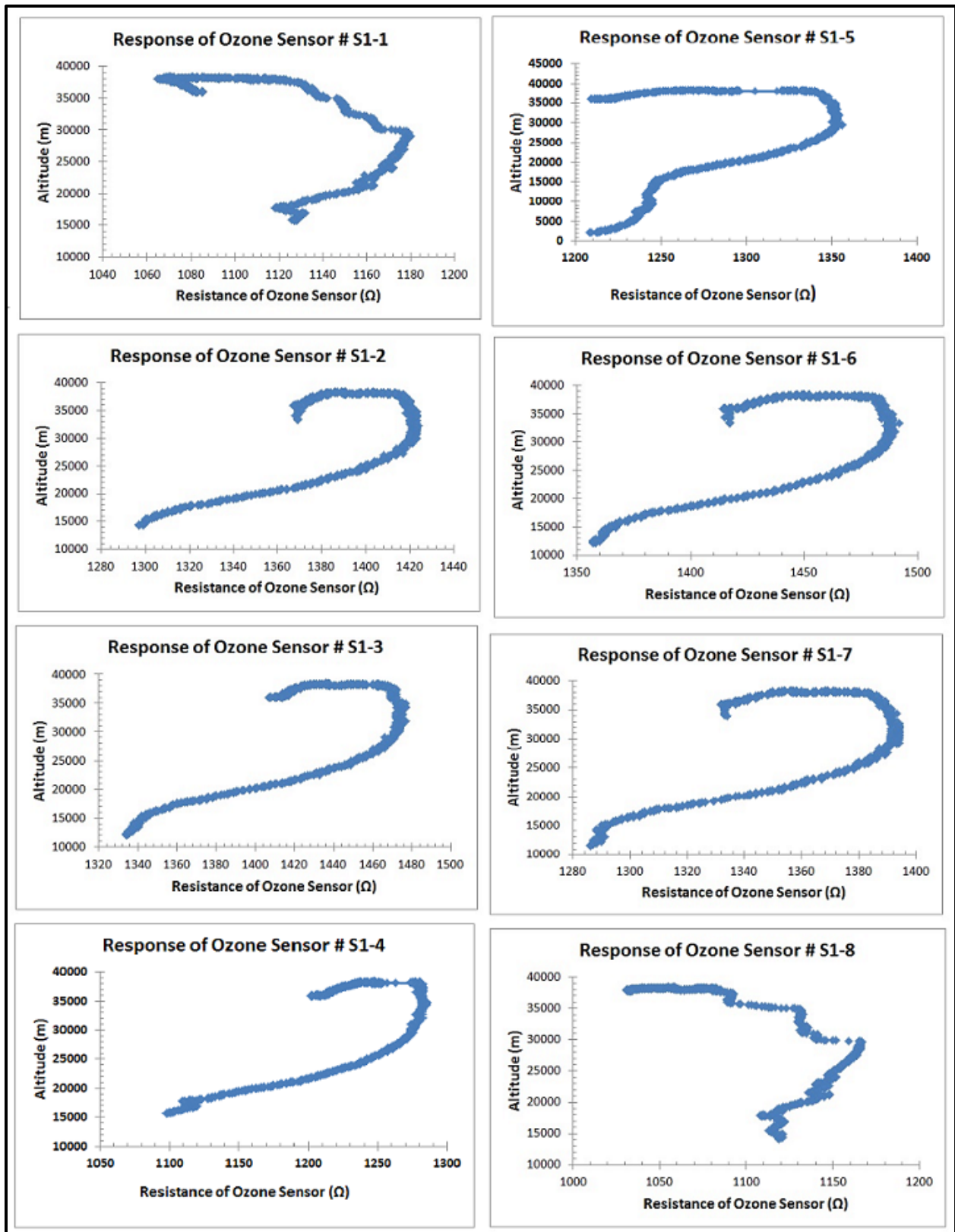


Fig.20 (a) Response of ozone sensors S1#1 to 8

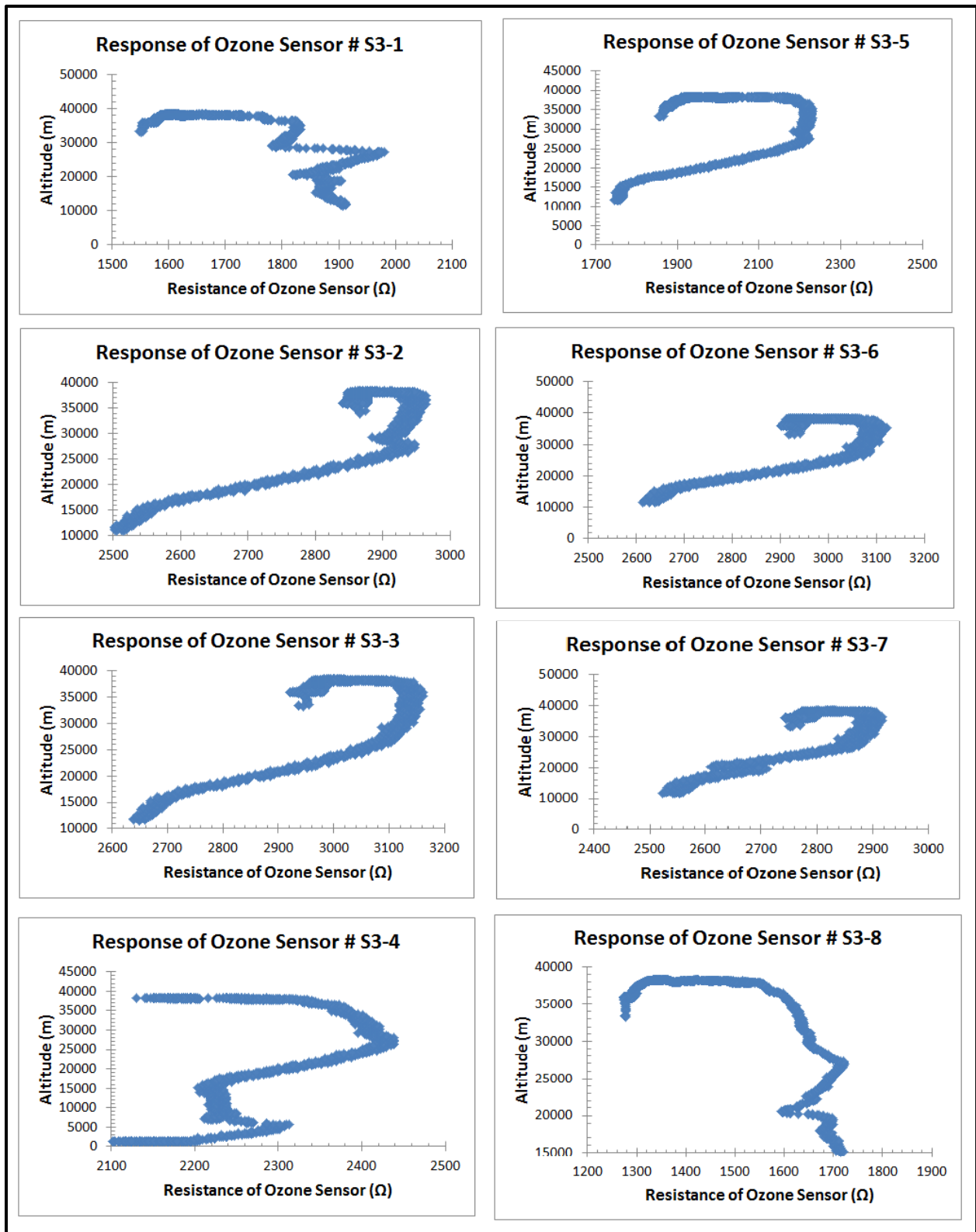


Fig.20 (b) Response of ozone sensors S3# 1 to 8

Both fig.20 (a) and (b) have shown the ozone peak in the stratosphere.

The response of sensors box #4 with altitude during ascending and descending of the flight is shown in fig. 20 (c). Note that these sensors did not respond with oxidizing ozone gas, but mainly with total mixture of reducing gases.

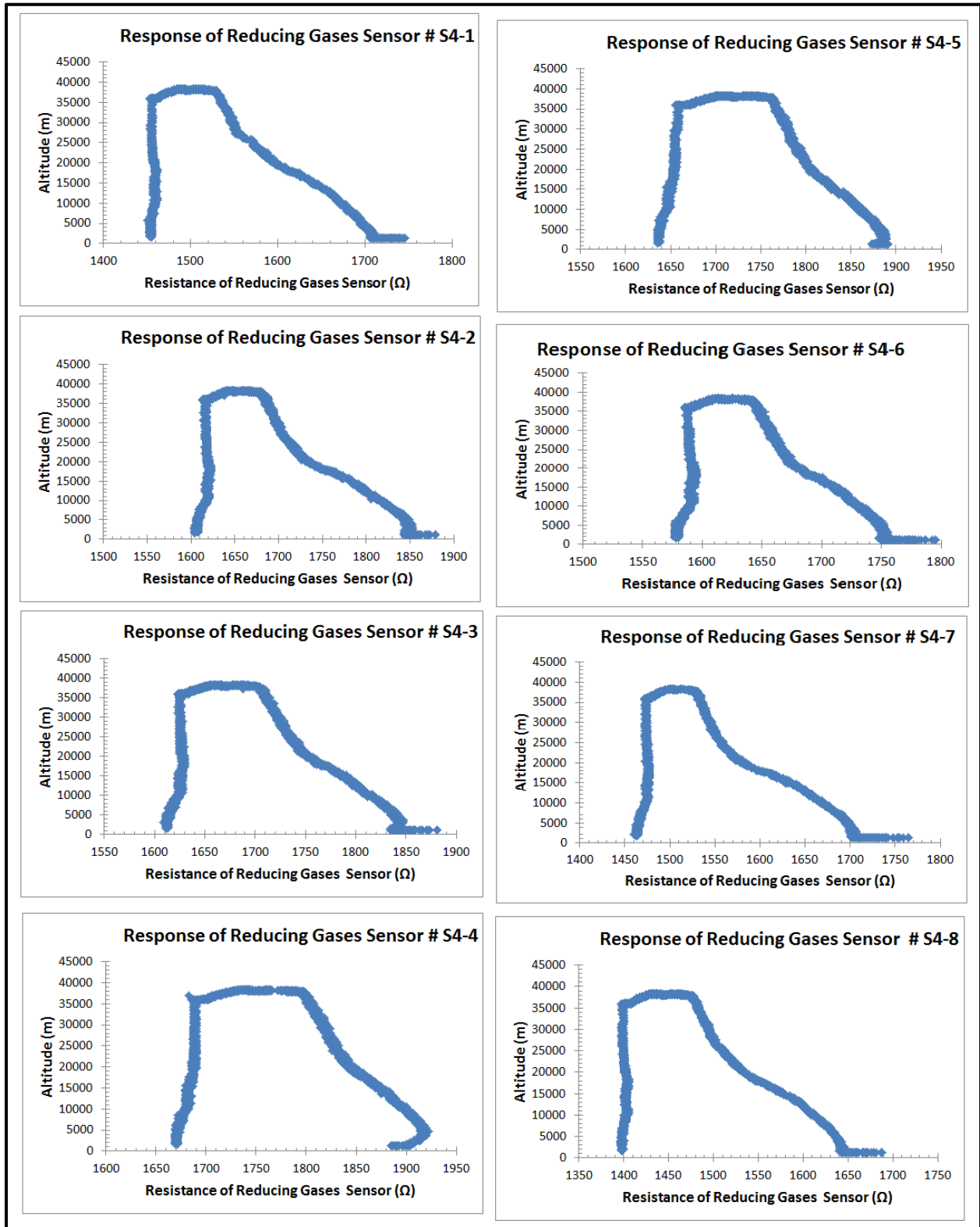


Fig. 20 Response of reducing gas sensors S4# 1 to 8

## 9.8 Measurements of ozone profile in the starosphere and comparison with the theoretical profile

Using calibration plots shown in fig. 7(a) and 7(b), the trend line equation of plot of each sensor was applied to convert the resistance values of the sensors into concentration of ozone gas in ppm.

Note that the calibration was made in low pressure, which can be applied mainly to starosphere range. It may not be good for atmosphere data. The ozone concentration measured from 0 to 10.0 ppm may have slight different value of slope and y intercept due to experimental error due to the variation of sensors thickness and leakage in the chamber.

The trend line equation of the calibration plot is given as:

$$y \text{ (sensor resistance, ohms) } = [m \text{ (slope). } x \text{ (concentration of ozone, ppm)}] + b \text{ (y intercept)}$$

$$\text{The concentration of ozone gas can be determined by: } x = (y - b)/m$$

The trendline equations for each sensors were listed in the following table-1.

Table-1 Trend line equations determined from the calibration plots shown in fig.7 (a) and (b) of gas sensors

Sensor Box # 1 (Using calibration plots shown in Fig.7(a))			
Concentration of Ozone (=x) (ppm)			
Sensor#		Sensor#	
S1-1	$x = (y-1059)/15.28$	S1-5	$x = (y-1209.6)/17.5$
S1-2	$x = (y-1299)/15.27$	S1-6	$x = (y-1359)/16.74$
S1-3	$x = (y-1339)/17.11$	S1-7	$x = (y-1280.4)/15.16$
S1-4	$x = (y-1140)/17.45$	S1-8	$x = (y-1032)/17.53$
Sensor Box#3 (Using calibration plots shown in Fig.7 (b))			
Concentration of Ozone (=x) (ppm)			
Sensor#		Sensor#	
S3-1	$x = (y-1820)/20$	S3-5	$x = (y-1960)/32.9$
S3-2	$x = (y-2840)/15.8$	S3-6	$x = (y-2910)/26.3$
S3-3	$x = (y-2945)/26.3$	S3-7	$x = (y-2760)/19.3$
S3-4	$x = (y-2206)/29$	S3-8	$x = (y-1595)/15.8$

With these equation parameters, we obtained the following the ozone profile plots shown in fig.21 (a) and (b):

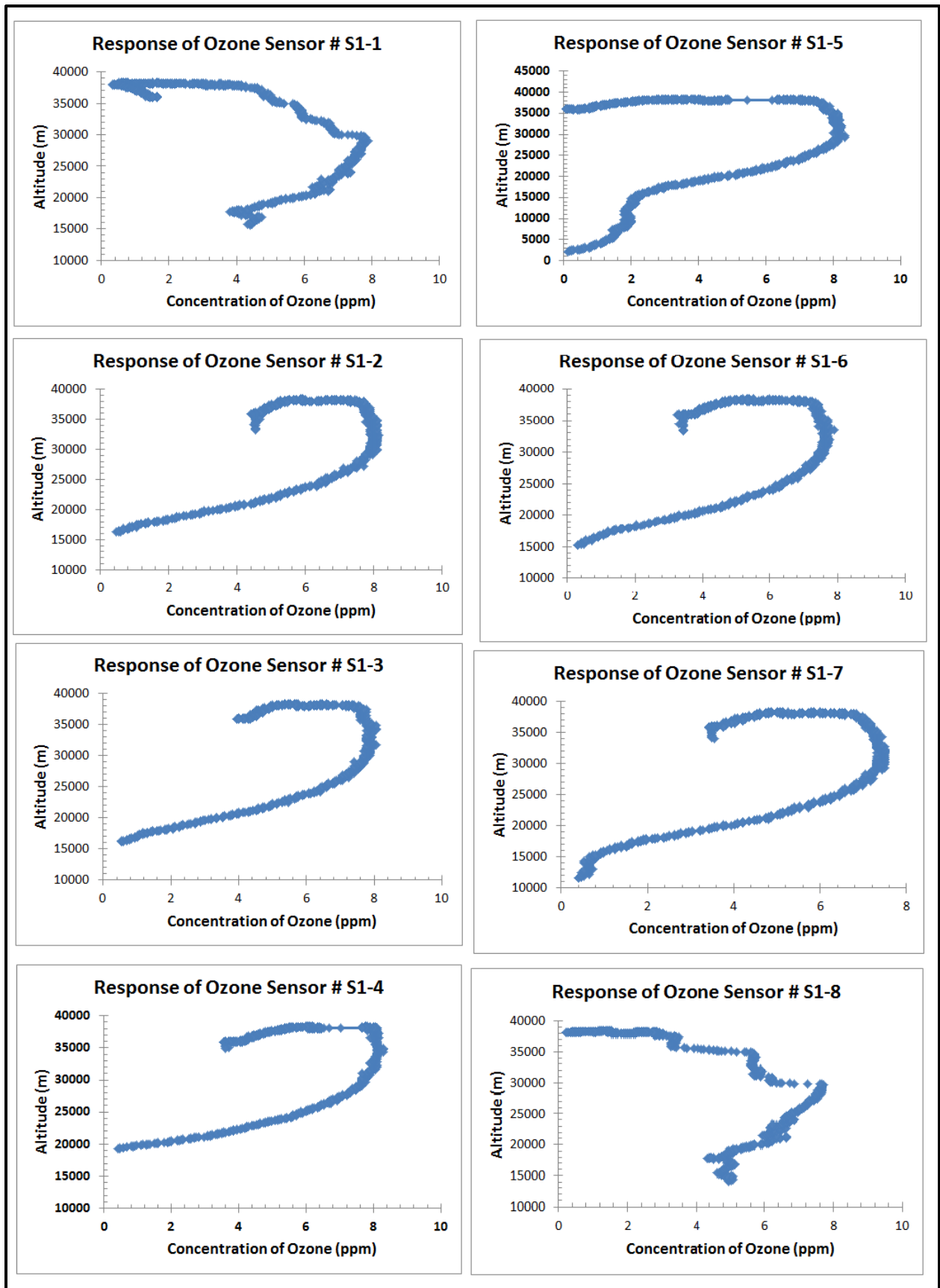


Fig 21(a) Ozone profile of sensors # S1-1 to S1-8

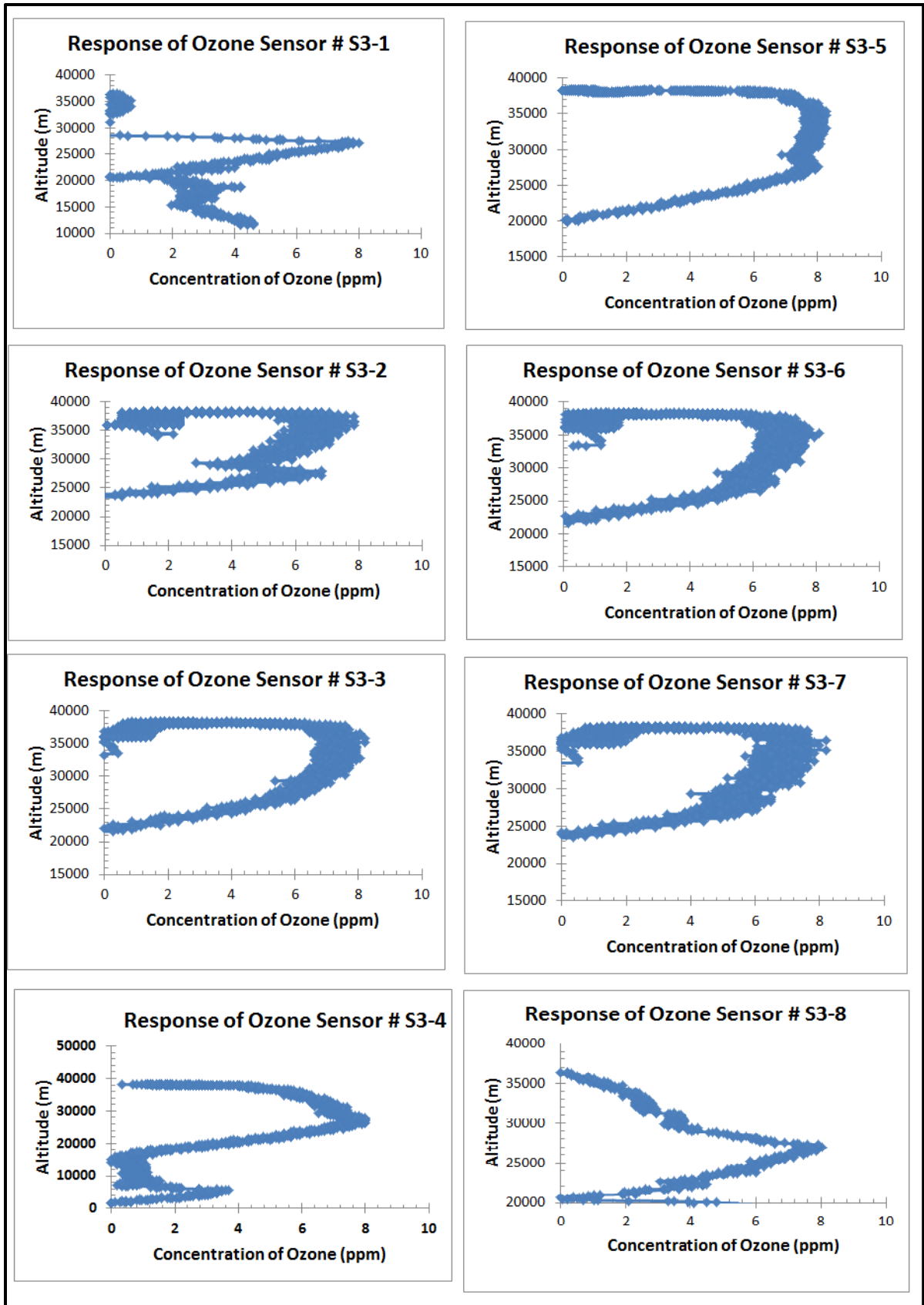


Fig 21(b) Ozone profile of sensors # S3-1 to S3-8

The nature of ozone profiles measured by ozone sensors box #1 and 3 are nearly matched with the theoretically profile measured and quoted by various research groups, which are shown in Fig. 23 to 26 for the comparison purpose. The measured value of maximum concentration of ozone was observed from 7.4 to 8.05 ppm, which is very close to the expected values. We will find out some theoretical calculation method to generate theoretical data for comparison.

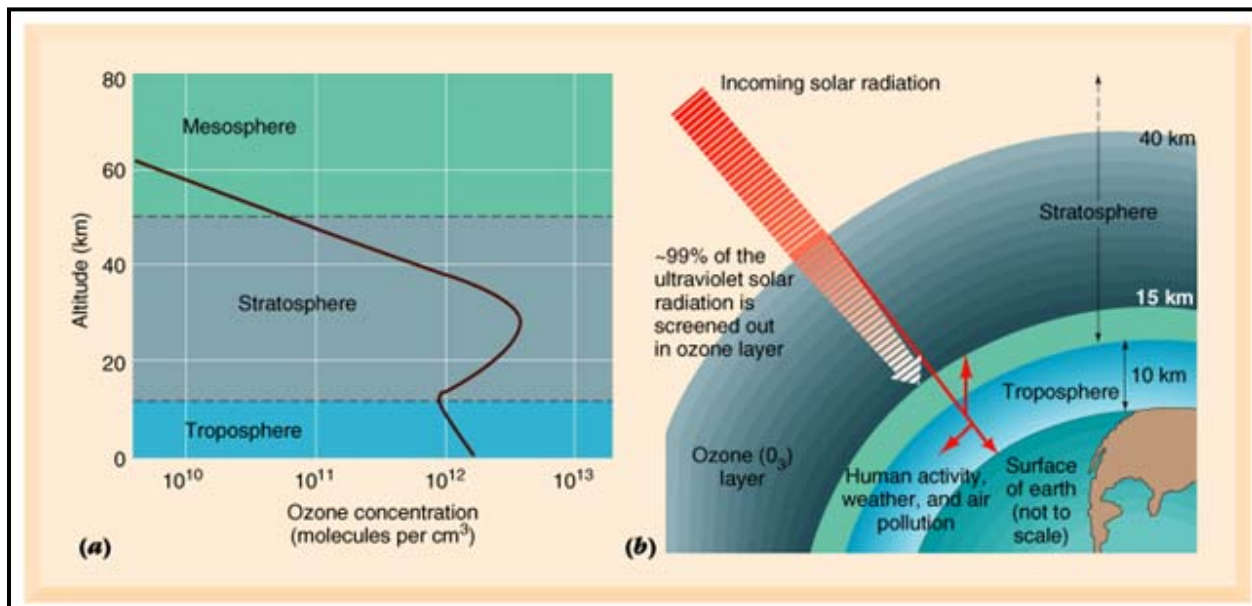


Fig.23 Ozone in the atmosphere

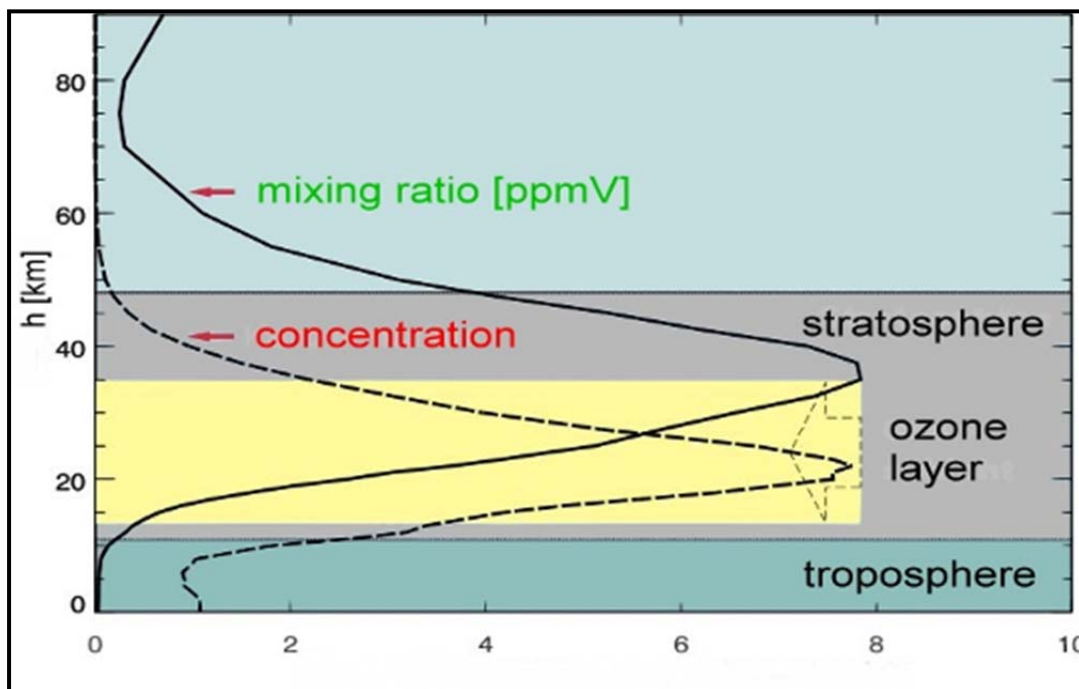
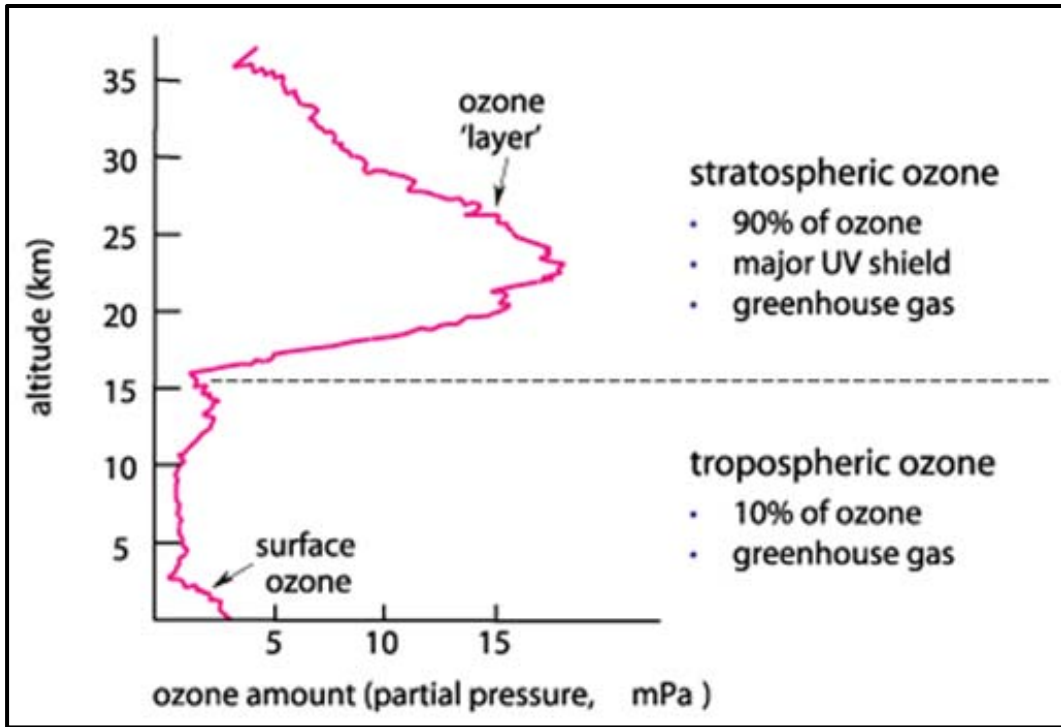


Fig.24 Theoretical ozone profile in stratosphere (<http://www.atmosphere.mpg.de/enid/1yy.html>)

(ppmv = parts per million by volume = volume mixing ratio)



<http://www.environment.gov.au/soe/2001/publications/theme-reports/atmosphere/atmosphere03-1.html>

Fig.25 Ozone in the atmosphere with its impact

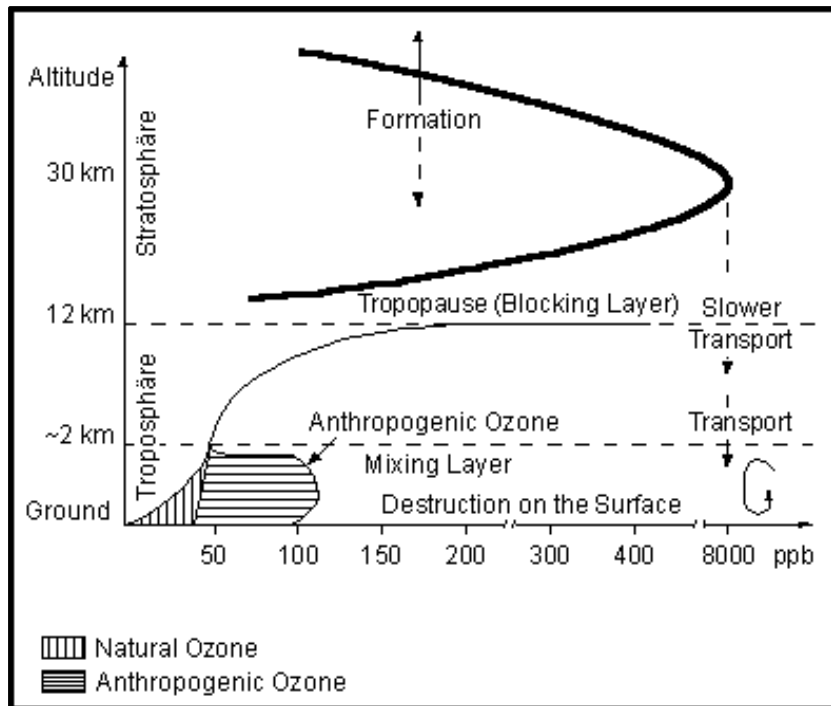


Fig.26 Ozone profile

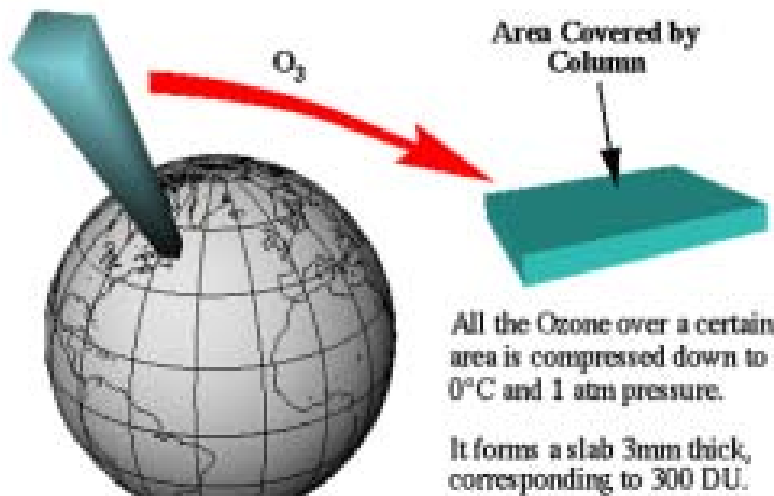
[http://www.stadtentwicklung.berlin.de/umwelt/umweltatlas/ed306\\_01.htm](http://www.stadtentwicklung.berlin.de/umwelt/umweltatlas/ed306_01.htm)

## Note: Units for measurement of ozone

In the presence study, we used part per million (ppm) units for determination of ozone concentration. We calibrated our sensors in the closed chamber using a digital ozone meter, which has unit in ppm only.

Ozone is mainly measured by the Dobson spectrometer in Dobson Units (DU). Our sensors are very cheap, smaller in size, low mass and easy to interface with electronic compared to that of Dobson spectrometer.

1 Dobson Unit (DU) is defined to be 0.01 mm thickness of gas at STP (0°C, 1 atm); the ozone layer represented above is then ~300 DU



Global Average Ozone: 300 DU=3 mm



Ozone Hole Average: 100 DU=1 mm



## 10. Problems, failure analysis and future plan

- (1) Pressure sensor was saturated at 110 mbar. We found that that pressure sensor can work only up to 110 mbar. We planned to replace it by new pressure sensor in the next flight.
- (2) Light sensors helped us to verify the science concept of generation of ozone in the presence of UV light. The data sheet indicated us that the spectral response was not larger in the UV light, but in near visible light. We planned to replace these light sensors by only UV light sensors.
- (3) Our nanocrystalline ozone gas sensors (Box # 1 and 3) worked well. Reducing gas sensors (box #4) shown good selectivity with ozone gas and did not responded with ozone gas. Reducing gas sensors worked reasonably well for detection of total reducing gases. We need to work further to distinguish different types of reducing gases and apply the calibration algorithm.
- (4) We did not able to add a radio circuit in the payload to communicate data in addition to HASP communication link in order to develop *a free flying payload*. This is because tight time schedule and limited budget. We will add it in the next flight.
- (5) We will add one external temperature sensor and humidity sensor mounted on outside of the payload body to measure ambient temperature and humidity.

## 11. Conclusions:

- (i) The improved nanocrystalline ITO thin film gas sensors (Box#1) and nanocomposite ZnO+ITO thin film gas sensors fabricated (Box#3) by the UNF team have good selectivity with ozone gas and worked well during entire flight period and measured the ozone profile of the stratosphere. Nanocomposite WO<sub>3</sub>+ITO thin film gas sensors (Box#4) have good response with total reducing gases and did not measured the ozone gas and hence shown good selectivity with ozone gas. The results of reducing gas sensors were better than that of the last year. Our science objectives of all these sensors were successfully tested and scientifically verified. We will modify the composition of WO<sub>3</sub>+ITO and make it better selectivity for different reducing gases and will use it to measure reducing gases in atmosphere and troposphere during next HASP2015 flight.
- (ii) Light sensor proved the presences of UV light, which are responsible to generate more ozone gas by converting oxygen into ozone.
- (iii) Improved temperature control circuit and software program gave better stability of temperature of sensors during entire flight period.
- (iv) New software handles all sensors data and faster conversion of RAW file into EXCEL file for quick view of the plots and also makes the real-time monitoring the plots using LabVIEW.

- (v) After recovery of payload, we tested the payload, circuit and all sensors and found all parts in good working condition.
- (vi) UND-UNF team is interested to make further improve sensors payload and seeking another opportunity for the HASP 2015 flight.

## 12. Acknowledgements

We are very grateful to

- (i) Dr. Gregory Guzik and Mr. Michael Stewart, HASP-LSU for their continue help, cooperation and encouragement. We also appreciate help of Mr. Doug Granger for his support.
- (ii) Columbia Scientific Balloon Facilities (CSBF)-NASA, Palestine TX and Fort Sumner, NM, and team of CSBF.
- (iii) Florida Space Grant Consortium for providing the financial support to UNF team.
- (iv) Dr Jaydeep Mukherjee, Director, Florida Space Grant Consortium (FSGC) and Ms. Sreela Mallick, FSGC for their valuable help and encouragement.
- (v) Websites links mentioned in this report for using their pictures to explain the science of this report. Our intention is not to violate any copyright, but only education and research purposes.

